

Order amidst disorder in semi-regular, tatty, and atypical random nanodevices with locally correlated disorder

M.A. Novotny*

*Department of Physics and Astronomy
HPC² Center for Computational Sciences
Mississippi State University
Mississippi State, MS 39762-5167[†]*

Tomáš Novotný

*Department of Condensed Matter Physics
Faculty of Mathematics and Physics
Charles University
Ke Karlovu 5
CZ-121 16 Prague, Czech Republic
(Dated: October 31, 2021)*

We make unexpected predictions for the electrical conductance and local density of states (LDOS) of a wide class of semi-regular nanodevices, tatty nanodevices, and nanodevices with atypical but arbitrarily strong disorder. Disorder is disruptive to electron transport, as it causes coherent electron scattering. Nevertheless, we predict a wide class of nanodevices which show order amidst disorder, in that the device Hamiltonians are disordered but when the device is attached to proper leads the LDOS is ordered. These nanodevices also are quantum dragons, as they have complete electron transmission, $\mathcal{T}(E) = 1$ for all electron energies which propagate in the attached leads. We analyze a conventional single-band tight-binding model by NEGF (Non-Equilibrium Green's Function) methods. We provide a recipe to allow extensive disorder in coherent transport through quantum nanodevices based on semi-regular, random, or tatty 2D, 3D, and 2D+3D underlying graphs with arbitrarily strong disorder in the tight-binding parameters, while the nanodevice keeps the desired quantum properties. The tight-binding parameters must be locally correlated to achieve order amidst disorder and $\mathcal{T}(E) = 1$. Consequently, in addition to the known regular examples of armchair single-walled carbon nanotubes and zigzag graphene nanoribbons, we predict a large class of metallic allotropes of carbon with $\mathcal{T}(E) = 1$. We also provide in two different regimes universal scaling analysis for the average transmission, $\mathcal{T}_{\text{ave}}(E)$, for nanodevices which have nearly the desired quantum properties.

I. INTRODUCTION

Materials should keep desired physical properties when made into a device. This is true for metallic quantum nanomaterials; they should keep the desired properties of having at least one extended (nonlocalized) state, and when proper leads are attached have complete electron transmission [$\mathcal{T}(E)=1$, for all electron energies E which propagate through the leads]. Here we study nanodevices with atypical but arbitrarily strong disorder which keep the desired metallic properties. Contrary to the common belief that disorder must always decrease $\mathcal{T}(E)$, we find a large class of metallic disordered nanodevices. This new class of metallic nanodevices spans the range from ones with strong but atypical disorder, ones with limited disorder but possessing a tatty structure, to ones

based on graphs with a semi-regular structure. This new class greatly expands the known metallic nanodevices, which include nanodevices with no disorder, such as the transitionally invariant cases of armchair carbon nanotubes and zigzag graphene nanoribbons. Even though the model systems have Hamiltonians with strong disorder and which lack translational invariance, they exhibit **order amidst disorder**, in that the local density of states (LDOS) of the propagating electrons is transitionally invariant. The new class of metallic nanodevices are found by insisting partitions of the device Hamiltonian all have a common structure (see App. A), with the device Hamiltonians based on an underlying (regular, semiregular, tatty, or disordered) graph in two dimensions (2D), 3D, or a combination 2D+3D. A graph is a mathematical construct comprised of vertices and edges which join two vertices [1]. In ball-and-stick models for materials, vertices are atom locations and edges are bonds between neighboring atoms. We restrict our analysis to graphs with N vertices which can be partitioned into ℓ slices. The bonds are restricted to being intra-slice bonds (both vertices in the same slice) or to being inter-slice bonds between vertices in neighboring slices.

Disorder is disruptive to electron transport, as it causes coherent electron scattering. The seminal work initiated

* man40@msstate.edu

[†] Also at

Department of Condensed Matter Physics
Faculty of Mathematics and Physics
Charles University
Ke Karlovu 5
CZ-121 16 Prague, Czech Republic

by Anderson [2, 3] showed in 1D materials models with short-range interactions that any amount of uncorrelated randomness gives that the wavefunction is exponentially localized. In the 1D case, long-range correlations in the disorder or long-range interactions in the Hamiltonian may produce extended states [4–7]. The existence of long-range correlations in the disorder, and the interplay between diagonal and off diagonal disorder [8], can lead to effective mobility edges and necklace states [9] which occur at particular energies and have $\mathcal{T}(E_{\text{necklace}}) \approx 1$.

In higher dimensions, the existence in some energy range of extended (not localized) states for linear operators with extensive disorder is an open problem in mathematical physics [10], one for which new results are presented in this paper. The scaling theory for typical disorder [11] for $D \geq 2$ suggests in 3D that for small enough uncorrelated typical disorder extended states almost surely occur, but for strong enough disorder the typical case is for only localized states to exist. 2D is a marginal dimension, as shown in [11] for the typical case there is no true metallic behavior, with decreasing $\mathcal{T}(E)$ exhibiting a crossover from logarithmic to exponential in the device length L . In this paper we study only *local* disorder correlations (atypical disorder), with an emphasis on the interplay of diagonal and off diagonal disorder, in 2D and 3D (and 2D+3D) models of nanodevices. For atypical disorder these nanodevices are shown to display the property of order amidst disorder and have complete electron transmission $\mathcal{T}(E)=1$.

We study electron transport and obtain the electrical conductance G (the electrical resistance is $R = 1/G$) of a model for a nanodevice. Uniform semi-infinite 1D thin leads are attached to the nanodevice. The leads have a hopping strength which we take to be our unit of energy, and have zero on site energy (defining our zero of energy). Therefore, electrons with energies in the range $-2 < E < 2$ can propagate in the leads (see App. B), and have a dispersion relation $\cos(q_{\text{lead}}a) = -E/2$ where a is the lattice spacing between atoms in the leads and q_{lead} is the wavevector of the electrons in the lead. When the leads are attached to the device, and connected at infinity to macroscopic reservoirs with slightly different chemical potentials, an electrical current flows through the device. We take the current flow in the device as being from slice j to $j+1$. The zero temperature, low bias electrical conductance G is related to the electron transmission $\mathcal{T}(E)$ at the Fermi energy E_F through the Landauer-Büttiker relations [12, 13]

$$G = \begin{cases} G_0 \mathcal{T}(E_F) & \xrightarrow{\mathcal{T}(E_F) \rightarrow 1} G_0 & \text{two probe} \\ G_0 \frac{\mathcal{T}(E_F)}{1-\mathcal{T}(E_F)} & \xrightarrow{\mathcal{T}(E_F) \rightarrow 1} \infty & \text{four probe.} \end{cases} \quad (1)$$

The quantum of conductance is $G_0 = 2e^2/h$ with e the electron charge, h Planck's constant, and the factor of two is due to the electron spin. Thus if the transmission is unity, in two probe measurements $G = G_0$, while in

four probe measurements the electrical resistance is zero ($R = 0$).

Because of the quantum nature of the device+leads problem, the electrical conductance in Eq. (1) is counter-intuitive. Nevertheless, both two-probe and four-probe results have been measured on the same nanodevice [14], a pure (no disorder) quantum wire which exhibits ballistic electron propagation because of the lack of scattering centers. For periodic metallic carbon systems with zero disorder, using a Bloch wave function or/and band structure approach theoretically gives $\mathcal{T}(E_F) = 1$. Theoretically and experimentally both single walled armchair carbon nanotubes and zigzag graphene nanoribbons have been shown to have the electrical conductance in Eq. (1) given by the maximum transmission $\mathcal{T}(E_F) = 1$ [15–20].

There are five important length scales for the discussion of electrical conductance in nanostructures. One is the lattice spacing a between atoms in a device (which we take to be the same as a in the leads), and another is the length L of the device along the direction of electron flow (which is proportional to the number of slices ℓ). Let the length a_{Dis} be the typical distance between uncorrelated disordered regions, where Hamiltonian parameters differ substantially. For any nanodevice the length scales a , a_{Dis} , and L are fixed after fabrication is complete. Introduce the additional energy-dependent length scale

$$\ell_{\mathcal{T}}(E) = \frac{L \mathcal{T}(E)}{1 - \mathcal{T}(E)}. \quad (2)$$

This length was used in Ref. [21] for the regime with $a \ll a_{\text{Dis}} \approx L$ as the effective elastic mean free path, the typical distance an electron travels before it scatters from the disorder. Strongly disordered devices have $a_{\text{Dis}} \approx a \ll L$, so the electron mean free path is ill defined, but we find the length in Eq. (2) still useful. There are three different well-studied regimes of length scales, as in Table I. The definition of ballistic is ‘relating to projectiles and their flight’, and for the regime with $a \ll L \ll a_{\text{Dis}}$ one can have $\ell_{\mathcal{T}} = \infty$ and loosely think of projectile motion of an electron moving in an ordered background of atoms because there are no disorder to scatter the electrons. As in Ref. [21], the diffusive regime is when $\ell_{\mathcal{T}} \ll L$, with the transmission very small due to the disorder scattering. Note $\ell_{\mathcal{T}}=L$ when $\mathcal{T}=1/2$, giving for a pure system the changeover between the ballistic and the diffusive transport regimes. Another length scale is the Anderson localization length ξ_A , where the overall shape of almost all wavefunctions is $\psi \sim \exp(-A/\xi_A)$ with A some constant. In the localized regime $\xi_A \ll L$. As the number of atoms in the device N increases, exponentially fewer wavefunctions span the nanodevice, thereby causing the transmission at almost all energies to be exponentially small. In both the diffusive and localized regimes there exist very narrow resonances, which become even narrower in energy as N increases, and these necklace states have been observed in 1D [9]. The ballistic, diffusive and localized regimes of length scales are well studied, and all relate to typi-

TABLE I. Lengths and regimes in quantum transport in 2D and 3D.

Ordered		$a \ll L \ll a_{\text{dis}} \ll \infty = \ell_{\mathcal{T}} = \xi_{\Lambda}$	Ballistic	$\mathcal{T}(E) = 1$	$-2 < E < 2$
Typical	disorder	$a \leq a_{\text{dis}} \ll \ell_{\mathcal{T}} \ll L \ll \xi_{\Lambda}$	Diffusive	$\mathcal{T}(E) \ll 1$	almost all E
Typical	disorder	$a \leq a_{\text{dis}} < \ell_{\mathcal{T}} \ll \xi_{\Lambda} \ll L$	Localized	$\ln(\mathcal{T}(E)) \ll 0$	almost all E
Atypical	disorder	$a \leq a_{\text{dis}} \leq L \ll \infty = \ell_{\mathcal{T}} = \xi_{\Lambda}$	Quantum Dragon	$\mathcal{T}(E) = 1$	$-2 < E < 2$

cal disorder or the lack of any disorder. In 1D models with weakly correlated short-range and long-range randomness effective mobility edges can be present [5]. In 1D models with correlated diagonal and off-diagonal disorder mobility edges can also be present [8].

This paper presents for the first time a new regime (see Table I) in 2D and 3D, and 2D+3D, nanosystems where with only *local* disorder correlations of the tight binding parameters the atypical disordered case with complete electron transmission, $\mathcal{T}(E) = 1$, is obtained. We restrict ourselves to 2D, 3D, and 2D+3D graphs with only short-range interactions. We introduce and study nanodevices in the fourth regime listed in Table I in this paper, namely nanodevices which have

$$a \leq a_{\text{dis}} \leq L \ll \infty = \ell_{\mathcal{T}}, \xi_{\Lambda} \quad (3)$$

and may have arbitrarily strong disorder but still have $\mathcal{T}(E) = 1$ for all $-2 < E < 2$ and order amidst disorder. We term these atypical disordered nanodevices quantum dragon nanodevices [22, 23]. All previous quantum dragon nanodevices had disorder correlated throughout the nanodevice, either all vertices within a slice had Hamiltonian parameters globally correlated, or each of the ℓ slices were identical. We show for the first time quantum dragon nanodevices exist for *extensive, locally correlated* tight binding parameters in 2D, 3D, and 2D+3D models of nanodevices. These atypical cases with locally correlated disorder contrast with the typical cases of disorder which gives the diffusive and localized regimes in Table I. As human history has shown, often it is the atypical materials which provide technological advances. Think of the difference between the use of a 1 kg inorganic typical material on earth, namely a rock, compared to 1 kg of iron. The difference is the difference between stone age technology and iron age technology.

The paper is organized as follows. In Sec. II the traditional tight binding Hamiltonian is described. Sec. III gives the method to obtain quantum dragon nanode-

vices for atypical disorder in the tight binding Hamiltonian. Sec. IV introduces the traditional NEGF (non-equilibrium Green's function) method we use to calculate the LDOS. Sec. V presents and tests our scaling analysis for nanodevices which are almost quantum dragons. Sec. VI analyzes nanodevices based on 2D hexagonal graphs, together with the proper cutting, sewing, braiding, twisting, printing, and associated combinations to ensure these devices are quantum dragons and exhibit order amidst disorder. Sec. VII presents quantum dragon nanodevices based on 2D rectangular and square-octagonal graphs. Sec. VIII presents strongly disordered quantum dragon nanodevices based on 3D hexagonal and 3D simple cubic graphs. Sec. IX shows order amidst disorder for nanodevices based on combination 2D+3D graphs. Sec. X includes our discussion and conclusions.

II. TIGHT BINDING MODEL

We study the standard single-band tight binding model, also sometimes called the Anderson model. We examine the model on a graph [1] of N vertices with edges which can be viewed as being in 2D, 3D, or 2D+3D. We assume the graph vertices can be partitioned into ℓ slices each with m vertices. Index the vertices within a slice by $i = 1, 2, \dots, m$ and the slices by $j = 1, 2, \dots, \ell$. We here restrict ourselves only to graphs with intra-slice edges (vertices with the same value of j) and inter-slice edges confined to being between vertices in slice j and in adjacent slices $j \pm 1$. As a model for materials, the graph vertices represent the locations of atoms, and the graph edges are hopping paths, often called bonds, for electrons between the atoms due to the electron wavefunction overlap of the two atoms labeled i, j and i', j' . We study only graphs which may represent actual nanomaterials, by limiting ourselves to $D \leq 3$ and short-range bonds. The Hamiltonian on the graph has the form

$$\mathcal{H} = \sum_{j=1}^{\ell} \sum_{i=1}^m \epsilon_{i,j} \hat{c}_{i,j}^{\dagger} \hat{c}_{i,j} - \sum_{\langle i,j;i',j' \rangle} t_{i,j;i',j'} \left(\hat{c}_{i,j}^{\dagger} \hat{c}_{i',j'} + \hat{c}_{i',j'}^{\dagger} \hat{c}_{i,j} \right). \quad (4)$$

The graph has $N = \ell m$ vertices (N atoms in the device), and each has an associated on site energy $\epsilon_{i,j}$. The cre-

ation (annihilation) operators are $\hat{c}_{i,j}^{\dagger}$ ($\hat{c}_{i,j}$). Every bond present has a hopping term of strength $t_{i,j;i',j'}$, and the

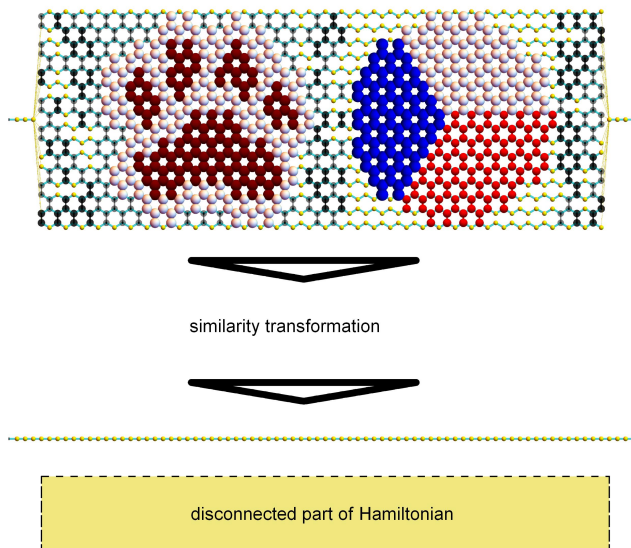


FIG. 1. Technique to show complete electron transmission for atypical strongly disordered nanosystems. See text in Sec. III for full description.

second sum is over all edges of the graph. Here we restrict our graphs so in 2D or 3D there are only nearest-neighbor (nn) or next-nearest neighbor (nnn) bonds. This nn and nnn restriction is not necessary [22] to find quantum dragons, but gives more physical quantum dragon nanodevices. We predict some of these quantum dragon nanodevices can be experimentally synthesized.

The tight binding model we study in Eq. (4) is the traditional model to study conductance through nanodevices. Although the model is a low-level approximation for actual materials, it nevertheless has been well studied and applied to understanding properties of materials. For example, with only nn hopping terms the tight binding model has been used to study π -orbital graphene nanoribbons [24], even though an *ab initio* method is preferable [25]. In this article we take the hopping to be a real number and study only zero external magnetic fields, however in general the hopping terms may be complex numbers. Most researchers study typical disorder, and models with locally-correlated but arbitrarily-strong disorder were expected to have $\mathcal{T}(E) \ll 1$ in 2D and 3D, as this is the diffusive or localized regimes. Nevertheless, we restrict our studies to quantum dragon devices, namely devices with strong atypical disorder but which have $\mathcal{T}(E)=1$ for all $-2 < E < 2$ and show order amidst disorder. Table I summarizes four different regimes for electron transmission through nanodevices.

III. METHODOLOGY TO OBTAIN QUANTUM DRAGON SOLUTIONS

Even knowing quantum dragon devices exist, the usual

theoretical tools of Bloch wavefunctions and band structure cannot be used, due to $a \sim a_{\text{Dis}}$ and hence even the wavevector in the disordered device is ill defined.[26] The way to find and analyze the atypical disordered cases which are quantum dragons is sketched in Fig. 1.

A. Finding dragons: General method

The Hamiltonian in Eq. (4) for an $m \times \ell$ graph is a $\ell m \times \ell m$ matrix \mathcal{H} . We perform a similarity transformation on \mathcal{H} , as depicted in Fig. 1, in order to block diagonalize the Hamiltonian. We study only atypical locally correlated disorder where this similarity transformation can be obtained. We have restricted ourselves to Hamiltonians which have a block-triangular structure, namely written for $\ell = 6$ slices the form is

$$\mathcal{H} = \begin{pmatrix} \mathbf{A}_1 & \mathbf{B}_{1,2} & \mathbf{0} & \mathbf{0} & \mathbf{0} & \mathbf{0} \\ \mathbf{B}_{1,2}^\dagger & \mathbf{A}_2 & \mathbf{B}_{2,3} & \mathbf{0} & \mathbf{0} & \mathbf{0} \\ \mathbf{0} & \mathbf{B}_{2,3}^\dagger & \mathbf{A}_3 & \mathbf{B}_{3,4} & \mathbf{0} & \mathbf{0} \\ \mathbf{0} & \mathbf{0} & \mathbf{B}_{3,4}^\dagger & \mathbf{A}_4 & \mathbf{B}_{4,5} & \mathbf{0} \\ \mathbf{0} & \mathbf{0} & \mathbf{0} & \mathbf{B}_{4,5}^\dagger & \mathbf{A}_5 & \mathbf{B}_{5,6} \\ \mathbf{0} & \mathbf{0} & \mathbf{0} & \mathbf{0} & \mathbf{B}_{5,6}^\dagger & \mathbf{A}_6 \end{pmatrix} \quad (5)$$

where each matrix is $m \times m$. We restrict our studied nanodevices so all ℓ intra-slice matrices \mathbf{A}_j (which contain all on site energies and all intra-slice hopping terms) as well as all $\mathbf{B}_{j,j+1}$ inter-slice matrices (which contain all inter-slice hopping terms) have a common eigenvector, \vec{v}_{Dragon} . Note the \mathbf{A}_j are Hermitian, while the $\mathbf{B}_{j,j+1}$ need not be Hermitian. In fact, the method will be generalized in Sec. IX so the $\mathbf{B}_{j,j+1}$ are not even square matrices. In the main text we will choose \vec{v}_{Dragon} to have every element equal to $1/\sqrt{m}$, which will be generalized in App. D.

The effect of the similarity transformation is depicted in Fig. 1. In the new basis one block of size $\ell \times \ell$ is the Hamiltonian of a uniform wire with ℓ sites, and only this part is connected to the external leads. In the main text, generalized in App. D, the similarity transform consists of the product of two unitary matrices. One unitary matrix \mathbf{X}_N consists of a block diagonal matrix with ℓ blocks each being a $m \times m$ discrete Fourier transform matrix, or Vandermonde matrix, with the k_1, k_2 element $\omega^{(k_1-1)(k_2-1)}/\sqrt{m}$ with the m^{th} root of unity $\omega = \exp(-i2\pi/m)$. The second unitary matrix \mathbf{P}_N is a permutation matrix which puts the first element of the k_3 $m \times m$ block into the k_3^{th} position, while shifting all other elements out of the first $\ell \times \ell$ matrix block. The resulting unitary similarity transformation matrix \mathbf{U}_N has a specific structure. The rectangular block submatrix of \mathbf{U}_N connecting the original site basis $\alpha \equiv \{i, j\}$ (with $i = 1 \dots m, j = 1 \dots \ell$) with the uniform wire part (labelled by $\eta = 1, \dots, \ell$) in the rotated basis is

$$(\mathbf{U}_N)_{\alpha,\eta} = \delta_{j,\eta}/\sqrt{m}, \quad (6)$$

see Sec. II and Fig. 4 in the Supplemental Material. We restrict ourselves to disorder which under the similarity transformation yields in the rotated basis a uniform wire as in Fig. 1, thereby giving a quantum dragon nanodevice with $\mathcal{T}(E) = 1$ and order amidst disorder.

The utilization of the symmetry transformation is sketched in Fig. 1 for a strongly disordered zigzag 2D hexagonal nanodevice with $\ell = 70$ and $m = 16$. The top of Fig. 1 shows the physical space nanodevice with the tight-binding parameters color and size coded. The sphere sizes are proportional to the on site energy values $\epsilon_{i,j}$, with the color code: (light gray, 0.7), (dark gray, 0.8), (red, 0.9), (cyan, 1.0), (white, 1.1), (maroon, 1.2), and (blue, 1.3). The bond radii are proportional to and use the same color code denoting the hopping strength $t_{i,j;i',j'}$. The exceptions are the yellow spheres that denote atoms with on site energy zero, and the yellow bonds which connect the device to the leads and have hopping strength $1/\sqrt{m}$. Using the similarity transformation described above (and in the supplemental material), the device Hamiltonian (a $\ell m \times \ell m = 1120 \times 1120$ matrix) of the top physical space depiction is changed to a different basis depicted pictorially on the bottom. For select atypical disorder, the Hamiltonian in the new basis is block diagonal, with the two blocks $\ell \times \ell = 70 \times 70$ and $\ell(m-1) \times \ell(m-1) = 1050 \times 1050$. The $\ell \times \ell$ block is a uniform 1D wire with $\ell = 70$ atoms, and is the only block of the Hamiltonian which is connected to the leads. The 1050×1050 block of the Hamiltonian is strongly disordered, but is disconnected from the leads and hence does not influence the electron transmission. The semi-infinite wires in physical space connect using hopping strengths \vec{v}_{Dragon} to the atoms in the end slices of the nanodevice, and hence are only connected to the uniform wire segment in the new basis. The real-space device attached to leads (top) as well as the connected 1D wire (bottom) both have $\mathcal{T}(E)=1$ for all $-2 < E < 2$, although intuitively only the bottom representation shows an obvious ‘short circuit’ behavior.

B. Finding dragons: Specific example

Consider a special case in order to illustrate the similarity transformation. This special case occurs for nanodevices based on 2D hexagonal (as in Fig. 1) and 2D square-octagonal graphs. We consider graphs with m vertices in every slice.

Since every slice has m atoms, all inter-slice matrices can be chosen to be $\mathbf{B}_{j,j+1} = -\mathbf{I}_{m \times m}$ with the $m \times m$ identity matrix being $\mathbf{I}_{m \times m}$. Hence for all $\mathbf{B}_{j,j+1}$ matrices \vec{v}_{Dragon} is a common eigenvector with eigenvalue -1 . This means the only inter-slice bonds are

$$t_{i,j;i',j'} = \delta_{i,i'} \delta_{j',j \pm 1}. \quad (7)$$

The eigenvalue of $\mathbf{B}_{j,j+1}$ is the value of the hopping term in the attached leads, so the uniform wire in the rotated basis in Fig. 1 is the same as the attached leads (where we

took the hopping value in the semi-infinite wires as our unit of energy). Note in Eq. (4) there is a negative sign put in, the same as for a uniform 1D wire as in App. B.

We consider the special case where every vertex has at most one intra-slice bond associated with it. For a 2D hexagonal device (as in Fig. 1), every atom is connected to at most one intra-slice bond. Whenever there is an intra-slice bond between atoms i, j and $i+1, j$, we need to ensure the uniform \vec{v}_{Dragon} is an eigenvector of \mathbf{A}_j with eigenvalue zero. Because there is at most one intra-slice bond per atom, we require for every intra-slice bond the condition

$$\begin{pmatrix} \epsilon_{i,j} & -t_{i,j;i+1,j} \\ -t_{i,j;i+1,j} & \epsilon_{i+1,j} \end{pmatrix} \begin{pmatrix} 1 \\ 1 \end{pmatrix} = \begin{pmatrix} 0 \\ 0 \end{pmatrix} \quad (8)$$

yields

$$\epsilon_{i,j} = \epsilon_{i+1,j} = t_{i,j;i+1,j}.$$

We need the eigenvalue of \mathbf{A}_j associated with \vec{v}_{Dragon} to be zero in order to make the uniform wire in the rotated basis in Fig. 1 be the same as the attached leads, and we chose our zero of energy as the value of the on site energy of the leads atoms. Equation (8) is satisfied for atypical disorder with the *local* correlation whenever an intra-slice bond is present.

It is important to stress Eq. (8) has only *local* correlations, as every intra-slice bond strength can be chosen independently from every other one, and furthermore is independent of m and of ℓ . In other words, one can independently assign any arbitrarily strong random value for $t_{i,j;i+1,j}$, make the on site energies satisfy the ‘dragon condition’ of Eq. (8), and have a device with order amidst disorder and $\mathcal{T}(E) = 1$.

IV. NEGF AND ORDER AMIDST DISORDER

We calculate the electron transmission $\mathcal{T}(E)$. $\mathcal{T}(E)$ is the probability of transmission of an electron to propagate to the end of the right lead (to $+\infty$) if it was injected with energy E from the end of the left lead (from $-\infty$). The transmission probability can be obtained from the solution of the time-independent Schrödinger equation for the infinite system of leads plus device. Alternatively it can be obtained by using standard NEGF methods [27–31] to obtain the same result using only matrices with the size of the Hamiltonian ($N \times N$). Alternatively, the electron transmission can be calculated using a related ansatz method [22, 23, 32, 33] for matrices of size $(N+1) \times (N+1)$. These two methods have been shown to be equivalent mathematically [23], as expected from physical considerations. The calculations in this paper used the NEGF method.

We consider a nanosystem, as in Eq. (4), with ℓ slices each with m atoms as in Eq. (5), so the number of atoms in the nanodevices is $N = m\ell$. We utilize the standard NEGF approach, wherein the transmission is given by

the trace over four $N \times N$ matrices [27, 29, 31] as

$$\mathcal{T}(E) = \text{Tr}(\mathbf{\Gamma}_L \mathcal{G} \mathbf{\Gamma}_R \mathcal{G}^\dagger). \quad (9)$$

The Green's function for an incoming electron with energy E is defined by

$$\mathcal{G}(E) = (E\mathbf{I} - \mathcal{H} - \mathbf{\Sigma}_L - \mathbf{\Sigma}_R)^{-1} \quad (10)$$

with the device Hamiltonian \mathcal{H} the $N \times N$ matrix from Eq. (4). Define $\xi = e^{-iq_{\text{Lead}}a}$, with q_{Lead} the wavevector in the leads. One has the dispersion relation in the leads

$$\cos(q_{\text{Lead}}a) = -\frac{E}{2}, \quad (11)$$

and consequently $\sin(q_{\text{Lead}}a) = \sqrt{4 - E^2}/2$. For our 1D leads, the self-energy for the incoming (left) lead is given by $\mathbf{\Sigma}_L = -\xi^* \vec{L} \vec{L}^\dagger$, with the N -dimensional vector \vec{L} having the first m elements from the vector \vec{v}_{Dragon} of hopping terms connecting the end atom of the incoming wire with the m atoms in the first slice of the nanodevice, and all other elements zero. Similarly, the self-energy for the outgoing (right) lead is given by $\mathbf{\Sigma}_R = -\xi^* \vec{R} \vec{R}^\dagger$ with the N -dimensional vector \vec{R} having all elements zero except the last m elements from the vector \vec{v}_{Dragon} of hopping terms connecting the end atom of the outgoing wire with the m atoms in the last slice of the nanodevice. The anti-Hermitian parts of the corresponding self energies are the broadening functions $\mathbf{\Gamma}_k = i(\mathbf{\Sigma}_k - \mathbf{\Sigma}_k^\dagger)$ for attached leads $k = L, R$. Once the transmission $\mathcal{T}(E)$ is calculated via the NEGF method of Eq. (9), the electrical conductance is given by Eq. (1).

From the NEGF, the LDOS at an energy E for each atom can be calculated in the standard fashion using

$$\text{LDOS}_{i,j}(E) = -\frac{1}{\pi} \text{Im}(\mathcal{G}_{i,j;i,j}(E)) \quad (12)$$

so only the diagonal elements of the imaginary part of the Green's function \mathcal{G} enter. It is important to realize that since the LDOS is calculated from the Green's function it is only for the propagating electrons. In other words, in Fig. 1(bottom) only the LDOS of the 1D wire part, not the disconnected part, gives $\text{LDOS}_{i,j}(E)$ in the physical space Fig. 1(top). We say a nanodevice exhibits **order amidst disorder** if it is disordered (the parameters $\epsilon_{i,j}$ and $t_{i,j;i',j'}$ are not all the same and/or are not in a regular pattern) while the $\text{LDOS}_{i,j}$ is ordered. The $\text{LDOS}_{i,j}(E)$ could be ordered or be in a regular pattern for all $-2 < E < 2$, thereby exhibiting order amidst disorder.

Order amidst disorder is illustrated by an example in Fig. 2, based on a nanodevice from a disordered 2D hexagonal graph. The nanodevice is a quantum dragon, with $\mathcal{T}(E) = 1$. Fig. 2(A) shows the left-hand portion of a strongly disordered nanodevice with $m = 16$, together

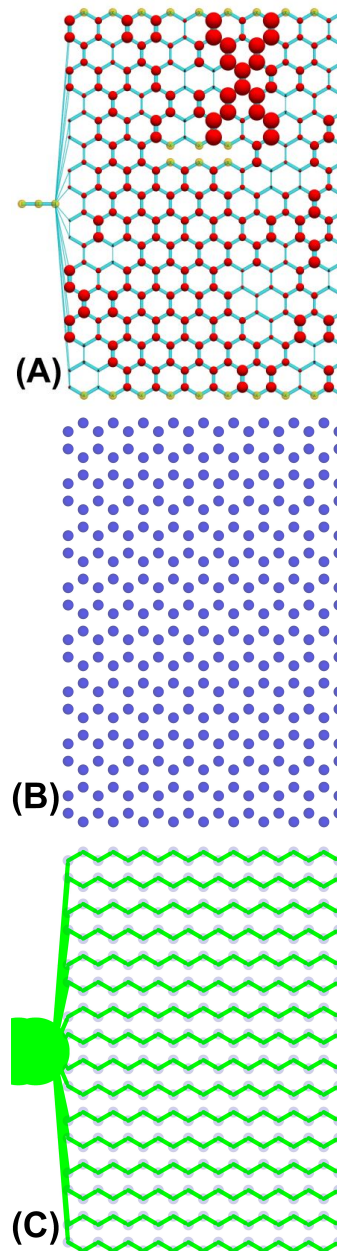


FIG. 2. Order amidst disorder, an illustration. (A) Shows the left portion of a disordered nanodevice with $m = 16$ based on a 2D hexagonal graph. (B) Shows the $\text{LDOS}_{i,j}(E)$ of the device in (A), which is ordered. (C) Shows the bond currents $I_{i,j;i',j'}(E)$ for the device in (A). Both (B) and (C) use energy $E = 1$, but the ordered LDOS and bond currents are present for any value of $-2 < E < 2$. See text in Sec. IV for full description.

with three atoms of the attached left-hand semi-infinite lead. All atoms with only two bonds have $\epsilon_{i,j} = 0$ (yellow spheres), the same as the lead atoms. The on site energies of other atoms are shown as red spheres with radii proportion to $\epsilon_{i,j}$. The hopping strengths are depicted as cyan cylinders with radii proportional to $t_{i,j;i',j'}$. All

non-vertical (inter-slice) bonds have $t_{i,j;i,j\pm 1} = 1$, the same as in the leads. The vertical (intra-slice) bonds were randomly chosen with $t_{i,j;i+1,j} \in [0.2, 1.5]$, the exception being a cut of three bonds ($t_{i,j;i+1,j} = 0$) to form two ribbons and the ‘X’ which is ‘printed’ just above the cut which has $t_{i,j;i+1,j} = 2$. From the values of $t_{i,j;i+1,j}$ the associated on site energies were chosen to satisfy the condition of Eq. (8), $\epsilon_{i,j} = \epsilon_{i+1,j} = t_{i,j;i+1,j}$, thereby ensuring $\mathcal{T}(E) = 1$ for any length ℓ of the device.

Fig. 2(B) shows the values of $\text{LDOS}_{i,j}(E)$ for each site (not shown for lead atoms) for the device in (A) at the energy $E = 1$. Note every site has the same LDOS, and so are represented by (blue) spheres with the same radii. This shows the concept of **order amidst disorder**, which is exhibited for any energy $-2 < E < 2$. In fact, our analysis in App. E (in particular Eq. (E12)) gives that for any quantum dragon with a uniform \vec{v}_{Dragon} one has

$$\text{LDOS}_{i,j}(E) = \frac{1}{\pi m \sqrt{4 - E^2}} \quad (13)$$

when the device has m atoms in each slice. Thus the lead atoms in Fig. 2(B) have an LDOS which is m times larger than the device $\text{LDOS}_{i,j}$.

Fig. 2(C) shows the local currents at $E=1$, superimposed on the $\text{LDOS}_{i,j}(E)$ from (B) for the nanodevice in (A). The green arrows have shaft radii proportional to the local bond current. The current in the lead splits evenly to flow in each of the m rows, with no vertical currents, again demonstrating **order amidst disorder**, and is exhibited for all $-2 < E < 2$. The NEGF method of calculating the bond currents is presented in Appendix C.

We also calculate the Density of States of the nanodevice, $\text{DOS}(E)$, in the normal box-counting fashion. Namely the Hamiltonian \mathcal{H} of Eq. (4) is diagonalized yielding N eigenvalues. The $\text{DOS}(E)$ is obtained by a box-counting method, namely counting the number of eigenvalues in a given interval ΔE that fall within the interval $[E - \frac{1}{2}\Delta E, E + \frac{1}{2}\Delta E]$. The DOS is calculated for the device without leads, while the LDOS is calculated once the leads are attached to the device. In the new basis after the similarity transformation, the DOS is calculated using both the wire and the disconnected part as in Fig. 1, while the LDOS is only determined by the portion connected to the leads. In terms of the mathematics, the LDOS is calculated from the Green’s function while the DOS is calculated from the Hamiltonian. This means for a quantum dragon the LDOS does not contain any contribution from the disconnected ‘pieces’, as in Fig. 1.

We stress the way we calculate the transmission, as well as both the LDOS and the local currents (see App. C), are by the normal NEGF formulas. For any size nanodevice and for any device Hamiltonian the calculations can in principle be performed, requiring only manipulations of $N \times N$ matrices. It is the precise form of the quantum dragon Hamiltonians, with their atypical disorder, which allow us to find $\mathcal{T}(E)=1$ for all $-2 \leq E \leq 2$, even

for extremely large N values. In fact, due to our similarity transformation comprised of two unitary matrices, for our atypical disorder it is much easier to calculate $\text{LDOS}_{i,j}(E)$ than it is to calculate $\text{DOS}(E)$. Namely, by utilizing the inverse of the two unitary matrices the $\text{LDOS}_{i,j}$ are proportional to i^{th} element of \vec{v}_{Dragon} , independent of j , for all ℓ slices. This is what leads to the order amidst disorder phenomena.

V. NEARLY QUANTUM DRAGONS

It is natural to ask what the transmission $\mathcal{T}(E)$ will be for nanodevices which have the tight binding parameters in Eq. (4) just slightly different from the tight binding parameters which give a quantum dragon nanodevice, i.e., what is the effect on a quantum dragon if the similarity transformation in Fig. 1 only approximately block diagonalizes the Hamiltonian. The underlying effects are shown in Fig. 3.

Fig. 3(A) shows a 2D hexagonal graph with $\ell = 12$ and $m = 4$, including some next-nearest-neighbor (nnn) inter-slice bonds. The intra-slice bonds and on site energies satisfy Eq. (8). All nnn inter-slice bonds were chosen randomly in $t_{i,j;i\pm 1,j+1} \in [0.0, 0.2]$ (or zero if $i-1 < 1$ or $i+1 > m$), and a quantum dragon would require every nn inter-slice hopping in every slice to satisfy

$$t_{i,j;i,j+1} = 1 - t_{i,j;i+1,j+1} - t_{i,j;i-1,j+1}. \quad (14)$$

The transformation \mathbf{U}_{12} would then yield a uniform wire segment connected to the leads, with the uniform wire segment in the new basis having all on site energies zero (the yellow cubes in the new basis) and hopping strengths uniform and equal to unity. In Fig. 3(A) the quantum dragon values for $t_{i,j;i,j+1}$ from Eq. (14) were instead randomly multiplied by a random number in $[0.5, 1.5]$. This added uncorrelated disorder gives a nanodevice which is almost a quantum dragon, and leads to weak hopping (with the sign of the hopping being either negative [black] or positive [red]) in the new basis between the sites which form the wire and the sites which are disconnected in a quantum dragon. This disorder also introduces different strengths of hopping in the rotated basis between adjacent wire nodes. These weak hopping terms in the new basis between the wire sites and previously disconnected sites lead to Fano resonances in the transmission [34].

More accurately, as seen in Fig. 3(B), there are Fano anti-resonances which suppress the transmission probability all the way to zero at particular energies. A Fano resonance [35] in electron transmission [34] depends on an asymmetry parameter q_{Fano} , a resonant energy E_{Fano} , and a resonant width Γ_{Fano} . The transmission can be

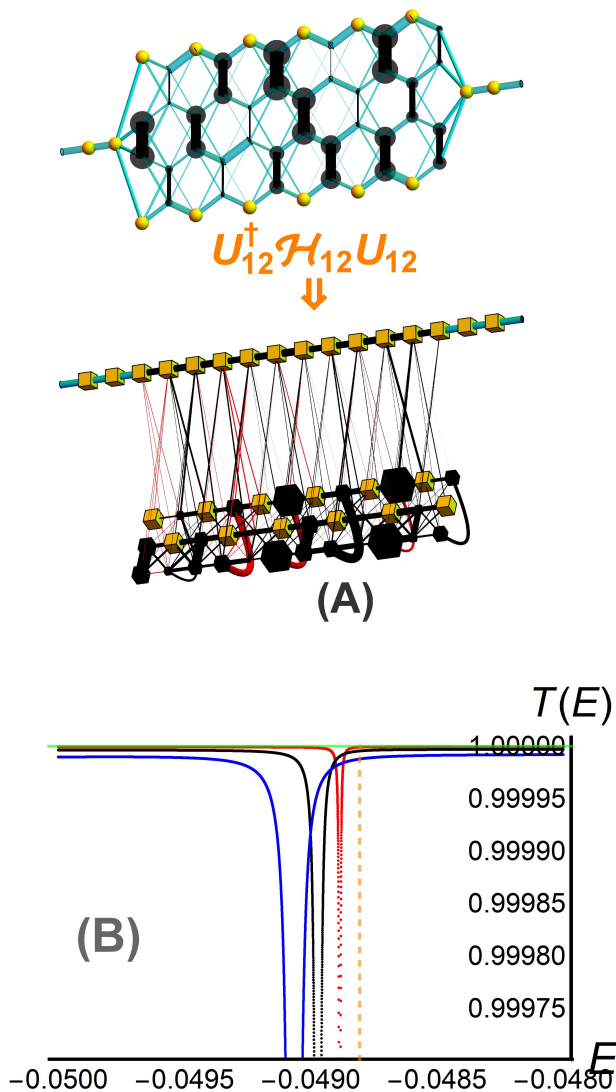


FIG. 3. The effect of the Hamiltonian of Eq. (4) almost being a quantum dragon. (A) A device based on a 2D hexagonal graph with $\ell = 12$ and $m = 4$, showing the effect of the unitary transformation \mathbf{U}_{12} on the device depiction when the device Hamiltonian is close to being a quantum dragon. (B) Shows $\mathcal{T}(E)$ for an example dragon device with $\ell = 80$ and $m = 22$ for four different strengths of uncorrelated disorder, $\delta = 0$ (green, $\mathcal{T}(E) = 1$ for all E), $\delta = 0.002$ (red), $\delta = 0.004$ (black), and $\delta = 0.006$ (blue). The dashed vertical orange line is the location of an eigenvalue of the $\delta = 0$ device Hamiltonian. All three finite δ values plunge to values numerically indistinguishable from zero. Note the expanded scales for E and $\mathcal{T}(E)$. See text in Sec. V for full description.

given by [34]

$$\mathcal{T}(E) = \frac{1}{1+q_{\text{Fano}}^2} \frac{(\epsilon_{\text{Fano}} + q_{\text{Fano}})^2}{\epsilon_{\text{Fano}}^2 + 1}$$

$$\epsilon_{\text{Fano}} = \frac{2(E - E_{\text{Fano}})^2}{\Gamma_{\text{Fano}}} \quad (15)$$

$$\text{extrema : } \begin{cases} \mathcal{T}_{\min} = 0 & \text{at } \epsilon_{\text{Fano}} = -q_{\text{Fano}} \\ \mathcal{T}_{\max} = 1 & \text{at } \epsilon_{\text{Fano}} = 1/q_{\text{Fano}} \end{cases}$$

which is bounded between zero and unity [36]. The locations of the (possible) resonance energies E_{Fano} for a material very close to being a quantum dragon with Hamiltonian $\mathcal{H}_{\text{Dragon}}$ are given by the eigenvalues of $\mathcal{H}_{\text{Dragon}}$ (at least within a tight binding approximation where the Hilbert space is of finite dimension). For a device with a single Fano resonance, when $|E - E_{\text{Fano}}|$ is large the transmission approaches $\mathcal{T} \rightarrow 1 - q_{\text{Fano}}^2$ for small q_{Fano} . When a very small amount of uncorrelated disorder is added to a quantum dragon, away from any given Fano resonance the transmission must approach unity as seen in Fig. 3(B). Hence a small but non-zero value for added disorder to a quantum dragon requires a small value for q_{Fano} . Hence in Fig. 3(B) $q_{\text{Fano}} \ll 1$, and the transmission goes to zero in line with Eq. (15).

Physically the uncorrelated disorder may be from a combination of slight differences in the hopping strengths (considered so far), in the onsite energies, or due to finite temperature effects (quenched phonons). The uncorrelated disorder of any origin causes Fano resonances with widths related to its strength δ [34], more accurately there are Fano anti-resonances which suppress the transmission probability all the way to zero at particular energies, while for small δ away from these resonance energies the transmission is $\mathcal{T} \approx 1$.

When averaging over the uncorrelated disorder the sharp Fano anti-resonances with perfect suppression of the transmission get fuzzy and the averaged transmission stays for a weak disorder strength δ close to 1, see Fig. 4 for purely onsite disorder. We can see that the three curves corresponding to different energies nearly collapse onto the same line for sufficiently weak disorder and only with its increasing strength they start to differ significantly.

This “universal behavior” for weakest disorder can be understood analytically by a simple lowest-order perturbation theory in the disorder strength δ , which is done in detail in Appendix E and results in the universal Eq. (E11) where the only appearing dragon parameters are the ℓ and m . No other details of a particular dragon setup enter. The energy dependence of the result is weak away from the band edges, and is determined solely by the uniform leads. This universal scaling for weakest disorder is shown in the inset in Fig. 4, which plots $\log_{10}(\delta)$ versus the scaling prediction of Eq. (E11) which should be equal to unity (the cyan horizontal line). Since $E = 1$

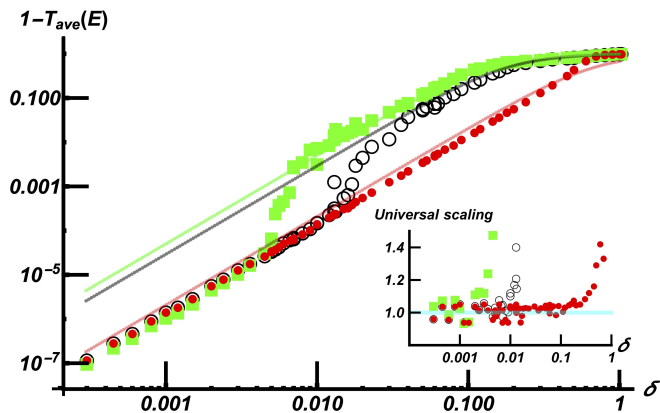


FIG. 4. The quantity $1 - \mathcal{T}_{\text{ave}}(E)$ vs δ is shown for a single quantum dragon based on a 2D hexagonal graph with $\ell = 80$ and $m = 20$ so $N = 1600$. The three energies shown are $E = -1, 0, 1$ shown as black, green, and red (open circles, squares, disks), respectively. The averages are over 10^5 different values of the uncorrelated disorder chosen from a Gaussian distribution with mean zero and width δ , with the random deviate chosen independently for each vertex and added to the on site energies of the quantum dragon values of that vertex. The lines show the predictions of Eq. (18) for the three energies. We see $1 - \mathcal{T}_{\text{ave}}$ is proportional to δ^2 , but exhibits a cross-over from averages dominated by a single nearby Fano resonance for small δ to the Eq. (18) prediction when the averages are due to many Fano resonances. The inset shows the universal scaling predicted in Eq. (E11) for very small δ . See text in Sec. V for full description.

is in a range with a very small $\text{DOS}(E)$ the Eq. (E11) universal scaling holds up to about $\delta \approx 0.2$.

With increasing disorder strength δ the situation dramatically changes and the transmission becomes strongly energy dependent. This corresponds to the regime of overlapping Fano anti-resonances and can be described by a scaling approach of Ref. [21] used for an analysis of doped silicon nanowires that have nearly ballistic electron transmission. Their analysis assumes the linear increase of the sample resistance with its length L , i.e., $\frac{1}{\mathcal{T}_{\text{ave}}(E)} = 1 + \frac{L}{l_e(E)}$. The mean free path for their system is $l_e(\epsilon_{\mathbf{k}}) = v(\epsilon_{\mathbf{k}})\tau(\epsilon_{\mathbf{k}})$, where the ballistic velocity of a propagating mode \mathbf{k} (relevant for the transmission and, thus, the conductance/resistance) $v(\epsilon_{\mathbf{k}}) = \sqrt{4 - \epsilon_{\mathbf{k}}^2}$ and the scattering time $\tau(\epsilon_{\mathbf{k}})$ is estimated from the Fermi golden rule for the scattering potential $\mathcal{V} = \sum_{\alpha} |\alpha\rangle v_{\alpha} \langle \alpha|$ with site-uncorrelated disorder potentials satisfying the condition (overbar denotes the impurity averaging) $\overline{v_{\alpha}} = 0$ and $\overline{v_{\alpha} v_{\beta}} = \delta^2 \delta_{\alpha\beta}$. For our quantum dragons, one has to be careful about using this formalism. For the case of nearly ballistic electron transmission of Ref. [21] the only scattering is due to the impurities, and because the system is almost pure the quantities $\epsilon_{\mathbf{k}}$ and $\tau(\epsilon_{\mathbf{k}})$, and hence $l_e(E)$ make sense in physical space. For a disordered quantum dragon the situation is more complicated to interpret. Only in the rotated basis, as depicted in Fig. 1, is a quasi-particle interpretation of $\epsilon_{\mathbf{k}}$ sensible,

and hence only in this not-physical-space basis can the quantities $v(\epsilon_{\mathbf{k}})$ and $\tau(\epsilon_{\mathbf{k}})$ be easily utilized. The calculation is

$$\begin{aligned}
 \frac{1}{\tau(\epsilon_{\mathbf{k}})} &= 2\pi \sum_{f \neq \mathbf{k}} \overline{|\langle \mathbf{k} | \mathcal{V} | f \rangle|^2} \delta(\epsilon_{\mathbf{k}} - \epsilon_f) \\
 &= 2\pi \langle \mathbf{k} | \overline{\mathcal{V} \delta(\epsilon_{\mathbf{k}} - \mathcal{H}) \mathcal{Q} \mathcal{V}} | \mathbf{k} \rangle \\
 &= 2\pi \sum_{\alpha, \beta} \overline{v_{\alpha} v_{\beta}} \langle \mathbf{k} | \alpha \rangle \langle \beta | \mathbf{k} \rangle \langle \alpha | \delta(\epsilon_{\mathbf{k}} - \mathcal{H}) \mathcal{Q} | \beta \rangle \\
 &= 2\pi \delta^2 \sum_{\alpha} |\langle \mathbf{k} | \alpha \rangle|^2 \langle \alpha | \delta(\epsilon_{\mathbf{k}} - \mathcal{H}) \mathcal{Q} | \alpha \rangle \\
 &= 2\pi \delta^2 \frac{1}{N} \sum_{\alpha} \langle \alpha | \delta(\epsilon_{\mathbf{k}} - \mathcal{H}) \mathcal{Q} | \alpha \rangle \\
 &\approx 2\pi \delta^2 \text{DOS}(\epsilon_{\mathbf{k}}),
 \end{aligned} \tag{16}$$

where the projector $\mathcal{Q} \equiv 1 - |\mathbf{k}\rangle \langle \mathbf{k}|$ and the DOS (per site) is defined as $\text{DOS}(\epsilon_{\mathbf{k}}) \equiv \frac{1}{N} \sum_{\alpha} \langle \alpha | \delta(\epsilon_{\mathbf{k}} - \mathcal{H}) | \alpha \rangle$. Neglecting the projector in the transition in the last line we have just neglected one out of N (eigen)states which should be a negligible error on the order of $1/N$. We have used the identity $|\langle \mathbf{k} | \alpha \rangle|^2 = 1/N$, which can be proven easily using the rotation matrix \mathbf{U}_N inserted into the scalar product $\langle \mathbf{k} | \alpha \rangle = \langle \mathbf{k} | \mathbf{U}_N \mathbf{U}_N^{\dagger} | \alpha \rangle$. Using the fact that the rotated propagating mode corresponds to an eigenstate of the uniform wire in the transformed basis and Eq. (6) we get

$$\begin{aligned}
 \langle \mathbf{k} | \mathbf{U}_N \mathbf{U}_N^{\dagger} | \alpha \rangle &= \sum_{\eta=1}^l \langle \mathbf{k} | \mathbf{U}_N | \eta \rangle \langle \eta | \mathbf{U}_N^{\dagger} | \alpha \rangle \\
 &= \langle \mathbf{k} | \mathbf{U}_N | j \rangle / \sqrt{m} \\
 &= \langle \mathbf{k}_{\text{wire}} | j \rangle / \sqrt{m} = e^{ikj} / \sqrt{lm}.
 \end{aligned} \tag{17}$$

Putting everything together we arrive at the following expression for the transmission in this regime

$$\begin{aligned}
 \mathcal{T}_{\text{ave}}(E) &= \frac{1}{1 + 2\pi \delta^2 L \frac{\text{DOS}(E)}{\sqrt{4 - E^2}}} \\
 \text{yielding} & \\
 \langle \text{DOS}(E) \rangle &= \frac{\sqrt{4 - E^2}}{2\pi \delta^2 L} \left(\frac{1 - \mathcal{T}_{\text{ave}}(E)}{\mathcal{T}_{\text{ave}}(E)} \right).
 \end{aligned} \tag{18}$$

Here the quotes on the ' $\text{DOS}(E)$ ' mean the scaling given by the right-hand side of Eq. (18) is an estimate under the assumptions required to obtain this scaling equation.

Both the regime with very small δ so $\ell_{\mathcal{T}} \gg L$ and the regime with $\ell_{\mathcal{T}} \approx L$ have $1 - \mathcal{T}_{\text{ave}}(E) \propto \delta^2$. The crossover can be understood by considering the effect of the Fano resonances [34] on the transmission. For $\delta \ll 1$ (namely $\ell_{\mathcal{T}} \gg L$) at a given energy E only the single closest Fano resonance contributes to decreasing $\mathcal{T}(E)$. For larger values of δ (namely $\ell_{\mathcal{T}} \approx L$), many Fano resonances at any energy E contribute to the decrease in $\mathcal{T}(E)$, leading to Eq. (18) which incorporates the DOS near E . Of course once δ is large enough so $\ell_{\mathcal{T}} \ll L$ one is very far from the dragon solution, and the diffusive regime predictions and eventually the 'gang of four' predictions [11] for the typical case of disorder are expected to hold.

Figure 5(A) shows the average transmission $\mathcal{T}_{\text{ave}}(E)$ for a quantum dragon nanodevice. The nanodevice is based on a 2D zigzag hexagonal ribbon with $\ell = 80$ and $m = 20$, with intra-slice bonds randomly chosen with $t_{i,j;i+1,j} = [0.5, 1.5]$ and associated on site energies chosen to satisfy $t_{i,j;i+1,j} = \epsilon_{i,j} = \epsilon_{i+1,j}$ so $\mathcal{T}(E) = 1$, shown as the green horizontal line. Each device has added to each on site energy of the quantum dragon Hamiltonian an additional random uniformly-chosen value in $[-\Delta_\epsilon, \Delta_\epsilon]$, and for the present intra-slice bonds a value chosen uniformly at random with $[-\Delta_t, \Delta_t]$. The analysis leading to Eq. (18) is only for random on site energies added to the dragon value, hence at first sight the analysis would have to be redone to take into account randomness in the bonds. However, because there is at most one most one intra-slice bond per atom, no matter the random value of the intra-slice bond it is possible to have the on site energy set to the dragon condition $\epsilon_{i,j} = t_{i,j;i+1,j} = \epsilon_{i+1,j}$. Furthermore, what enters Eq. (18) is only the variance δ^2 of the uncorrelated disorder. We need to relate the variance δ^2 with the variance from the dragon condition. The uniform probability distributions are $d\kappa_t/2\Delta_t$ and $d\kappa_\epsilon/2\Delta_\epsilon$. This gives the calculation for atoms with an intra-slice bond of the variance from the dragon condition

$$\frac{1}{4\Delta_t\Delta_\epsilon} \int_{-\Delta_t}^{\Delta_t} d\kappa_t \int_{-\Delta_\epsilon}^{\Delta_\epsilon} d\kappa_\epsilon (\kappa_t - \kappa_\epsilon)^2 = \frac{\Delta_\epsilon^2 + \Delta_t^2}{3}. \quad (19)$$

We choose $\Delta_t = \Delta_\epsilon = \Delta$, and so what enters into Eq. (18) is $\delta^2 = 2\Delta^2/3$. Furthermore, due to the hexagonal nature of the graph one has $L = \sqrt{3}la/2$. (These values are the lowest order terms as they neglect edge effects, but should be appropriate for comparison with our statistics.) Figure 5(B) shows the scaling of the same data as (A) using Eq. (18). With no adjustable parameters, Figure 5(B) shows excellent agreement with Eq. (18), with the three chosen values $\Delta = 0.08, 0.16, 0.24$ shown as red, black, blue, respectively. The transmission at each point is the average over 10^4 different realizations of the uncorrelated Gaussian-distributed on site parameters added to the quantum dragon value at that site. Also shown as green symbols is a box counting result of the average DOS(E) per site from 10^4 such $\Delta = 0$ random quantum dragon Hamiltonians. This scaling should be reasonably good for any quantum dragon nanodevice in an intermediate regime of δ . It should be reasonable for δ values smaller than when $\ell\mathcal{T}(E)$ of Eq. (2) is comparable to or larger than $L/2$, which some of the blue symbols in Fig. 5(B) are on the border of satisfying. It should also be reasonable if δ is not too small, in which case the universal scaling of Eq. (E11) is applicable.

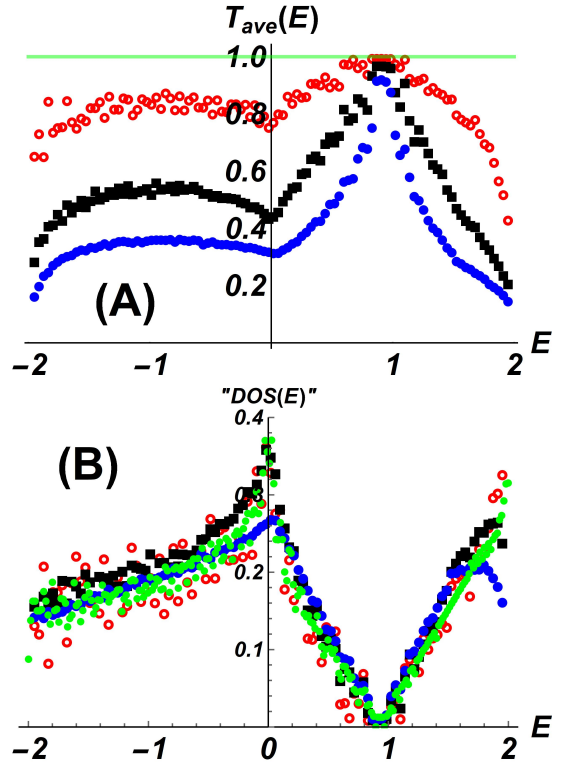


FIG. 5. A 2D hexagonal graph of an Eq. (4) Hamiltonian, with additional Gaussian-distributed uncorrelated on site energies added so the device is almost a quantum dragon. (A) shows the average transmission $\mathcal{T}_{\text{ave}}(E)$ versus energy for four values of additional on site energy, $\Delta = 0, 0.08, 0.16, 0.24$ shown as green, red, black, and blue, respectively. (B) Shows the same data as (A) scaled as in Eq. (18) for red, black, and blue symbols. The green is the result of a box-counting of the average DOS(E) from quantum dragon Hamiltonians ($\delta=0$) with 10^4 different $t_{i,j;i+1,j} = [0.5, 1.5]$ realizations. The scaling uses $L = \sqrt{3}la/2$ and $\delta^2 = 2\Delta^2/3$, so there are no adjustable parameters. See text in Sec. V for full description.

VI. ORDER AMIDST DISORDER: 2D HEXAGONAL GRAPHS

Regular pure lattices (zero disorder) of atoms in carbon nanotubes and graphene nanoribbons have an underlying 2D hexagonal graph.[37] The graphene nanoribbons (GNR) are based on segments of graphene, and a single-walled carbon nanotube (SWCNT) can be constructed by placing additional bonds in a regular fashion to connect atoms on the boundary of a GNR. Here we focus on a zigzag GNR as in Fig. 1 and Fig. 2 (which you must imagine with all device $\epsilon_{i,j}$ equal and all device $t_{i,j;i+1,j}$ equal). For our different carbon nanodevices we do not analyze whether or not they are stable (either chemically so they have the global minimum energy for all allotropes of carbon with N atoms, or kinetically so the energy is a local minimum with barriers greater than Boltzmann's constant times the absolute temperature). However, some of our predicted metallic allotropes may

be as stable as GNRs or SWCNTs. We obtain a large number of metallic nanodevices which have $\mathcal{T}(E)=1$ for $-2 < E < 2$, including the known regular pure nanodevices of armchair SWCNTs and zigzag GNRs. For an armchair SWCNT or zigzag GNR $L = \sqrt{3}(\ell - 1)a/2$ relates the physical device length to the number of slices ℓ in the underlying graph.

A regular pure (zero disorder) armchair SWCNT or zigzag GNR have translational invariance (at least along the direction of current flow), and hence have been analyzed using band structure and Bloch wavefunction techniques. However, both can also be analyzed with the described similarity transformation in Sec. III, in particular for the special case in Sec. III.B. Nature has regular pure armchair SWCNTs and zigzag GNRs satisfying Eq. (8) for device on site values $\epsilon_{i,j} = 1$ since all bonds (both inter-slice and intra-slice) are identical and can be chosen to have strength $t_{i,j;i',j'} = 1$ (by choosing the hopping strength of the attached semi-infinite leads to be the actual carbon-carbon bond hopping strength). Thus the method of analysis sketched in Fig. 1 is an alternative analysis to obtain ballistic transport in regular pure armchair SWCNTs and zigzag GNRs.

The critical lesson is that the analysis sketched in Fig. 1 does not require translational invariance. Hence it will allow us to find semi-regular, tatty, and strong atypical disordered nanodevices based on 2D hexagonal graphs. In other words, we will predict carbon-based quantum dragon nanodevices based on proper graph manipulations, including proper cutting, printing, sewing, braiding, twisting, and associated combinations. In all subsections for 2D hexagonal graphs, except Sec. VI.A, we take all $t_{i,j;i',j'} = 1$ (both intra-slice and inter-slice bonds), and take $\epsilon_{i,j} = 1$ if the atom has an intra-slice bond and $\epsilon_{i,j} = 0$ if the atom does not have an intra-slice bond. These are exactly the values one needs to obtain ballistic transport via the analysis of Sec. III for regular armchair SWCNTs and regular zigzag GNRs. Thus we predict a new large class of metallic carbon allotropes ranging from semi-regular to very tatty structures, all being metallic since they all have $\mathcal{T}(E) = 1$ for $-2 < E < 2$. All nanodevices in this section, except possibly Sec. VI.A, have very physically reasonable values for the on site energies and hopping terms within the tight binding model, as illustrated by the existence and stability of armchair SWCNTs, zigzag GNRs, and high strain carbon allotropes [38]. All of our predicted carbon allotropes will exhibit order amidst disorder, as in Fig. 2.

A. Graphene Nanoribbons: Cutting and Printing

In Fig. 1 and Fig. 2 we have already shown 2D hexagonal graphs illustrating printing and cutting. The point is that Eq. (8) must hold *locally* for each intra-slice bond hopping strength and the on site energies of the two atoms which share this bond. It is the local nature which allows for printing and cutting. Another exam-

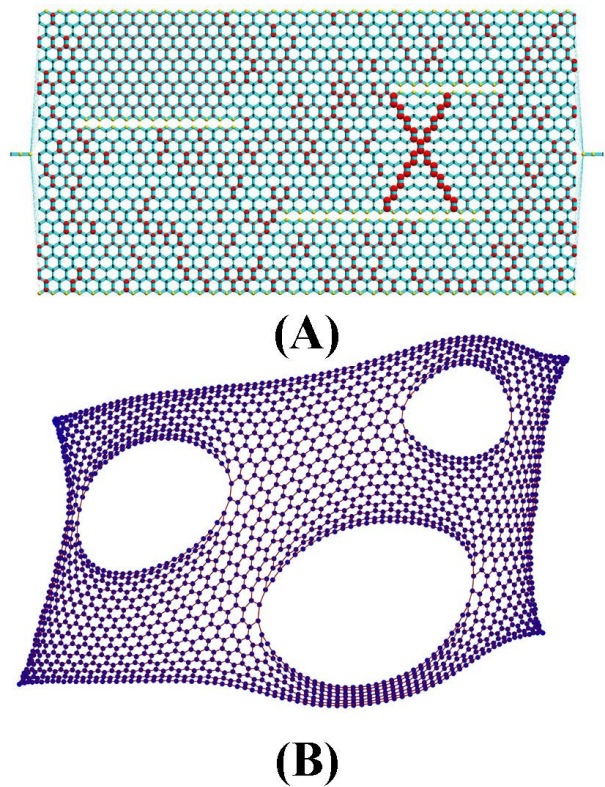


FIG. 6. Quantum dragon from a 2D hexagonal graph with $\ell = 81$ and $m = 25$. The same graph is shown in (A) and (B), with different graphing methods. See text in Sec. VI.A for full description.

ple of printing and cutting is shown in Fig. 6. In printing the values of the bond/site combinations are chosen to form a pattern. Printing does not change the underlying graph, it just weights the vertices and edges of the graph differently. Any intra-slice bond can also be cut by choosing $t_{i,j;i+1,j} = 0$ and the associated on site energies $\epsilon_{i,j} = \epsilon_{i+1,j} = 0$. Cutting deletes an edge which was present in the underlying graph.

Fig. 6 gives a further illustration of allowed printing and cutting of quantum dragon nanodevices based on 2D hexagonal graphs. Most intra-slice bonds were chosen uniformly at random to have strength $t_{i,j;i+1,j} \in [0.2, 1.5]$. The exceptions are: the printed ‘X’ which has $t_{i,j;i+1,j} = 2$ and the region around the ‘X’ which has $t_{i,j;i+1,j} = 0.1$; the three horizontal cuts with $t_{i,j;i+1,j} = 0$; and the region above the left-most cut which has $t_{i,j;i+1,j} = 1$. All device on site energies were then chosen to satisfy Eq. (8). Fig. 6(A) shows the zigzag ribbon nanodevice, with two atoms of each semi-infinite lead attached. The radii of all cyan cylinders are proportional to the hopping strength for that bond. The radii of the red spheres are proportional to $\epsilon_{i,j}$, while the yellow spheres depict on site energies of zero. In or-

der to better show the underlying graph, Fig. 6(B) utilizes the Mathematica [39] command `GraphPlot3D` utilizing the `SpringElectricalEmbedding` method of plotting, thereby better illustrating the underlying structure of this planar graph (note the structure is not optimized to be a minimum of the energy of a carbon nanodevice). No lead atoms are shown in Fig. 6(B). The graph is no longer regular (it is a graph rather than a lattice), and the parameters of the Hamiltonian are disordered (with locally correlated disorder). Fig. 6 forms an example of atypical disorder exhibiting order amidst disorder and $\mathcal{T}(E) = 1$.

B. Graphene Nanoribbons: Sewing

Sewing (or stitching) refers to adding a bond to an existing graph. In order to preserve the quantum dragon nature of the device, we must perform the sewing in an allowed fashion which keeps \vec{v}_{Dragon} as an eigenvector of all \mathbf{A}_j intra-slice matrices with associated eigenvalue zero and of all $\mathbf{B}_{j,j+1}$ inter-slice matrices with associated eigenvalue unity.

Any bonds can be added to any intra-slice matrix \mathbf{A}_j , with proper adjustment of the on site energies for any \vec{v}_{Dragon} with all elements non-zero. To show this, break \mathbf{A}_j into the sum of its diagonal part \mathbf{D}_j which contains only the on site energy values and its off-diagonal part $\tilde{\mathbf{A}}_j$ which contains its intra-slice hopping terms. A quantum dragon requires $\mathbf{A}_j \vec{v}_{\text{Dragon}} = \vec{0}$, which is $(\mathbf{D}_j + \tilde{\mathbf{A}}_j) \vec{v}_{\text{Dragon}} = \vec{0}$, which requires that one assign the on site energies such that

$$\mathbf{D}_j \vec{v}_{\text{Dragon}} = -\tilde{\mathbf{A}}_j \vec{v}_{\text{Dragon}}. \quad (20)$$

Thus sewing within each slice can be performed independently of other slices, and as long as every element of \vec{v}_{Dragon} is non-zero it is possible to adjust the on site energies to make the device a quantum dragon with $\mathcal{T}(E) = 1$ and order amidst disorder.

Fig. 7 shows the effect of sewing on a carbon allotrope. This can be viewed as a stitched zigzag ribbon, yielding a split armchair nanotube. Here \vec{v}_{Dragon} has all elements the same, all hopping strengths are equal to unity, and all on site energies are either unity in the bulk or zero on the edges. Fig. 7 starts with a 2D hexagonal graph, a GNR with $\ell = 120$ and $m = 26$, which has one cut in the middle portion, as in Fig. 7(A). In Fig. 7(A) sewing is done only in slices near the ends which have the two end on site values of zero, forming an unphysically long bond between the edges of the GNR while changing the edge on site energy values from zero to unity. This type of stitching requires m to be even. The Mathematica [39] command `GraphPlot3D` utilizing the `SpringElectricalEmbedding` method gives the more physical carbon allotrope in Fig. 7(B).

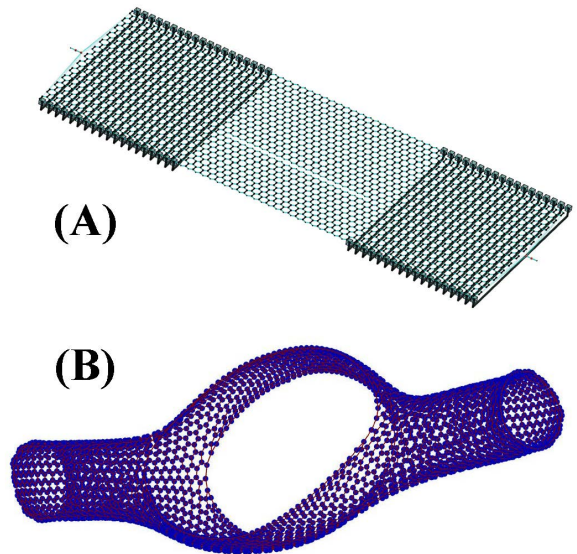


FIG. 7. Semi-regular quantum dragon allotrope of carbon, based on a 2D hexagonal graph with $\ell = 120$ and $m = 26$. The same graph is shown in (A) and (B), with different graphing methods. See text in Sec. VI.B for a full description.

If we had started with an even m zigzag GNR of length L and stitched every possible slice as above, we would end up with an armchair SWCNT of length L . Both the zigzag GNR and armchair SWCNT are stable even to high temperatures. For example, CVD-grown graphene nanoribbons have been annealed with temperatures up to 2800°C [40], where the high temperature annealing causes stitching between the edges of different nanoribbons. Molecular dynamics simulations of SWCNTs and multi-walled carbon nanotubes showed reasonable chemical stability even at 3000 K [41], and combined experimental and density functional theory (DFT) show SWCNTs stable in a nitrogen atmosphere to at least 1000 K [42]. Furthermore, one way to experimentally obtain very pure GNRs is to split a SWCNT [43–45] which is the opposite technique to stitching. Hasegawa [45] has also experimentally demonstrated the joining (stitching or sewing) of GNRs and carbon nanotubes. Fig. 7(B) is just the incomplete splitting of an armchair SWCNT. Therefore, one expects the structure in Fig. 7(B) to be stable. Our prediction is that it is also a semi-regular example of a quantum dragon, and should have $\mathcal{T}(E) = 1$ and hence metallic behavior even though the cut and edges provide a scattering mechanism of the transmitted electrons.

C. Graphene Nanoribbons: Twisting

Another proper manipulation of zigzag GNRs to keep them as a quantum dragon is twisting of ribbons formed by cutting a zigzag GNR or an armchair SWCNT. Such

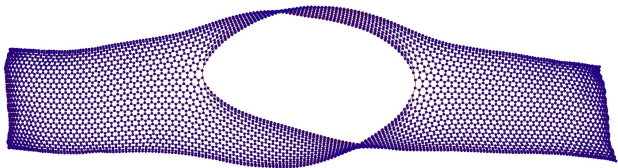


FIG. 8. Semi-regular quantum dragon Möbius strip allotrope of carbon, based on a 2D hexagonal graph with $\ell = 200$ and $m = 26$. See text in Sec. VI.C for full description.

twisting does not change the overall transmission at the single band tight binding model level, but can be performed to give for example a Möbius strip nanodevice. However, for carbon devices the hopping is due mainly to the pi orbitals perpendicular to the GNR. Therefore, twisting will install a phase change by $e^{i\pi}$ in the transiting electron path length compared to an untwisted ribbon. Eq. (21) illustrates the interface one must have between \pm and \mp regions of the nanodevice as the half twist of a Möbius strip is performed.

$$\begin{array}{cccccccccccc}
 \cdots & \pm & \pm & \pm & \pm & \pm & \mp & \mp & \mp & \mp & \mp & \cdots \\
 \cdots & \pm & \pm & \pm & \pm & \pm & \mp & \mp & \mp & \mp & \mp & \cdots \\
 \cdots & \pm & \pm & \pm & \pm & \pm & \mp & \mp & \mp & \mp & \mp & \cdots \\
 \cdots & \pm & \pm & \pm & \pm & \pm & \mp & \mp & \mp & \mp & \mp & \cdots
 \end{array} \quad (21)$$

Thus where the twisted ribbon is connected to the outgoing ribbon the hopping term is not -1 as it is everywhere else in the carbon device but $+1$ due to inclusion of the $e^{i\pi} = -1$ phase. Alternatively, the phase could be placed where the twisted ribbon is connected to the incoming electron ribbon, or somehow broken up over the slices where the ribbon is twisted with the sum of the phases along the twisted ribbon being π . The similarity transformation still gives a 1D wire in the rotated basis, but the 1D wire now has different hopping terms, but which all have the absolute value of unity. As shown in App. B, such phases in the hopping terms of a 1D wire have no effect on the transmission probability $\mathcal{T}(E)$. Therefore, we predict a Möbius strip zigzag GNR will be a quantum dragon.

Fig. 8 shows the Mathematica [39] command `GraphPlot3D` utilizing the `SpringElectricalEmbedding` method applied to a 2D hexagonal graph with $\ell = 200$ and $m = 26$ in a Möbius strip configuration. A cut is made from slices $j = 72$ to $j = 133$ yielding the middle part with two ribbons of widths 10 and 16, each of which have a half twist. Note for complete transmission it is not important whether both half-twists are counter-clockwise, clockwise, or one of each, the device will still be a quantum dragon.

If only one graphene ribbon had a half twist, the path lengths of the electrons along the two paths would be different, with an associated phase difference $e^{i\pi}$. The device would then have Fabry-Pérot oscillations. The same

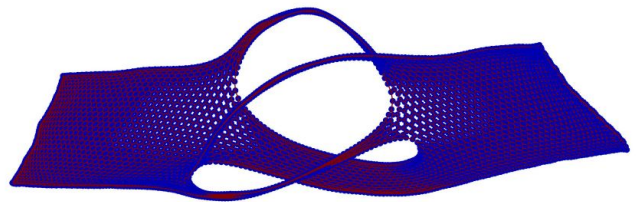


FIG. 9. Semi-regular quantum dragon allotrope of carbon illustrating braiding, based on a 2D hexagonal graph with $\ell = 200$ and $m = 30$. See text in Sec. VI.D for full description.

is true, with a different phase, if the two cut ribbons had different numbers of slices (different lengths). These types of Fabry-Pérot oscillations have been measured experimentally in a SWCNT, in which case the SWCNT-electrode coupling was important to understanding the nanodevice behavior [46].

In 2002 a single crystal which was a Möbius strip was synthesized [47]. There have been numerous theoretical works showing the stability and properties of GNRs which are Möbius strips [48–52]. Thus it is expected carbon nanodevices as in Fig. 8 will be stable. Here we make the prediction such Möbius GNRs should be metallic, and have $\mathcal{T}(E) = 1$ when properly connected to leads. The proper connections may be easier to achieve experimentally by having an armchair SWCNT as ends, using the stitching method of the previous section.

D. Graphene Nanoribbons: Braiding

Cuts of a zigzag GNR between slices j_1 and j_2 can be done to form many different ribbons. If k ribbons are cut between slices j_1 and j_2 , one can imagine at slice j_2 these ribbons are cut from the wide GNR which extends from $j_2 + 1$ to ℓ (which we call the exiting nanoribbon). The cut ribbons may then be reattached to the wide exiting nanoribbon in the same order. The ribbons may, however, be permuted in their order before reattaching to the wide exiting nanoribbon. Some of these permutations will braid the cut ribbons. A 2D hexagonal graph structure will remain, with all atoms having either three or two bonds and all smallest loops in the lattice hexagons, if all k ribbons are of even width. Before the cut ribbons are reattached to the exiting nanoribbon, they may be braided in many ways to form a regular or a random intertwining 3D arrangement. This braiding does not affect the quantum dragon property of the nanodevice.

Fig. 9 shows an example of braiding. The device has $\ell = 200$ and $m = 30$, with all device bonds of strength unity. Start with a zigzag GNR with $k = 4$ ribbons cut between slices $j_1 = 72$ and $j_2 = 134$. The top and bottom (as seen from the left-hand wide ribbon) cut ribbons have widths of 6, and the middle ribbons have widths of 4

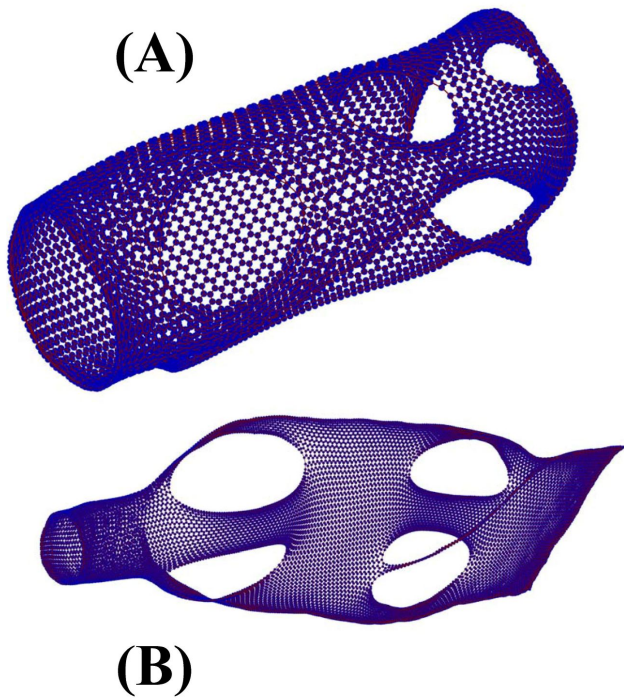


FIG. 10. Tatty quantum dragon allotropes of carbon illustrating combinations of cutting, sewing, twisting, and braiding (see text in Sec. VI.E). **(A)** Based on a 2D hexagonal graph with $\ell = 100$ and $m = 50$, with cuts between slices $23 \leftrightarrow 40$, $56 \leftrightarrow 70$, and $82 \leftrightarrow 92$. The three cuts between slices have ribbons with widths (10, 40), (16, 34), and (10, 24, 16), respectively. Both tube ends and two cut ribbons are stitched into nanotubes. **(B)** Based on a 2D hexagonal graph with $\ell = 300$ and $m = 50$, with cuts between slice $69 \leftrightarrow 128$ and $186 \leftrightarrow 241$. The first cut ribbons have widths (18, 20, 12) while the second cut ribbons have widths (14, 4, 18, 14). Only the left-hand end is stitched into a nanotube.

and 12. Before the cut ribbons are reattached to the exiting nanoribbon, they undergo the permutation in their attachment numbers of $(1, 2, 3, 4) \rightarrow (3, 1, 4, 2)$. Thus the two width 6 cut ribbons are attached to the exiting wide ribbon as the middle two ribbons. This braiding does not affect the transmission, as we still find $\mathcal{T}(E) = 1$ and an ordered $\text{LDOS}_{i,j}(E)$ for all $-2 < E < 2$. The GNR device in Fig. 9 could either be viewed as having a semi-regular structure with a lot of disorder or as a tatty structure.

E. Graphene Nanoribbons: Combinations

The allowed manipulations to keep an underlying 2D hexagonal graph as a quantum dragon nanodevice can be used in combinations. Assume we utilize a \vec{v}_{Dragon} with all elements the same, and keep the maximum graph co-

ordination number at three. Assume all hopping terms are equal to unity (or have an $e^{i\pi}$ phase for twisting), hopping terms are confined to nearest-neighbor bonds, and every atom has at most one intra-slice bond. Atoms with one (zero) intra-slice bond(s) have an on site energy of unity (zero). Then any allowed manipulations, including

- **Proper intra-slice cutting:** Setting any intra-slice hopping so $t_{i,j;i+1,j} = 0$, and associated on site energies $\epsilon_{i,j} = \epsilon_{i+1,j} = 0$;
- **Proper intra-slice printing:** Setting any value for $t_{i,j;i+1,j}$ and setting $\epsilon_{i,j} = \epsilon_{i+1,j} = t_{i,j;i+1,j}$;
- **Proper intra-slice sewing:** Adding a bond between any two atoms which have zero intra-slice bonds, and changing the associated on site energies to the dragon condition.
- **Proper ribbon twisting:** Twisting cut ribbons; even adding a reconnection phase if done properly;
- **Proper ribbon braiding:** Braiding in any fashion a sequence of cut nanoribbons;

can be used to form a nanodevice with $\mathcal{T}(E) = 1$ and order amidst disorder.

These combinations can make very strange looking nanodevices, but all will show order amidst disorder and $\mathcal{T}(E) = 1$. Two examples of tatty nanodevices based on an underlying 2D hexagonal graph are shown in Fig. 10, Figure 10**(A)** is based on a tattier graph than Fig. 9, while Fig. 10**(B)** is the tattiest of these three quantum dragon nanodevices.

VII. ORDER AMIDST DISORDER: OTHER 2D GRAPHS

Order amidst disorder can also be found starting with other 2D graphs. In this section we show results starting from square-octagonal graphs and rectangular graphs. Of course, just as with the 2D hexagonal graph, these graphs can also have appropriate cutting, sewing, braiding, twisting, and combinations thereof, all while still exhibiting order amidst disorder and $\mathcal{T}(E)=1$.

A. 2D quantum dragons: Square-octagonal graphs

Fig. 11 shows results for a disordered square-octagonal graph. For the square-octagonal graph use of Eq. (8) is appropriate because we utilize a \vec{v}_{Dragon} with every element equal to $1/\sqrt{m}$ and there is at most one intra-slice bond attached to any atom. Every intra-slice bond, and the associated on site energies, must satisfy Eq. (8) in order for the nanodevice to exhibit order amidst disorder and having complete electron transmission for all energies $-2 \leq E \leq 2$. If an intra-slice hopping is chosen to

be $t_{i,j;i+1,j}=0$, the bond is cut (being absent from the graph).

Fig. 11(A) shows a nanodevice based on a square-octagonal graph with 10% of the intra-slice bonds cut, chosen in a completely random manner. The remaining intra-slice bonds were chosen uniformly to be in $t_{i,j;i+1,j} = [0.8, 1.2]$. Fig. 11(B) shows the underlying graph for (A), without leads, with this graph representation more clearly showing the cut bond locations. For no added disorder, the device is a quantum dragon with $\mathcal{T}(E)=1$, and shows order amidst disorder (not shown) as the LDOS $_{i,j}(E)$ is uniform (independent of i and j) throughout the nanodevice for any $-2 < E < 2$.

Fig. 11(C) shows both the quantum dragon transmission (light green horizontal line $\mathcal{T}(E) = 1$), as well as the transmission averaged over 10^3 different values of additional Gaussian-distributed uncorrelated on site disorder with disorder strengths $\delta = 0.02, 0.04, 0.06$ corresponding to red, black, and blue points respectively. Fig. 11(D) replots the same values for the average transmission, but scaled according to Eq. (18), with the same color coding as in (C). Also shown (dark green) is the DOS(E) for the underlying graph shown in (B), with the points averaged over the number of eigenvalues of the device Hamiltonian \mathcal{H} using a box-counting method with $\Delta E = 0.1$. With no adjustable parameters, the comparison with our theory of Eq. (18) is very good, unless one gets too close to the band edges at $E = \pm 2$.

B. 2D quantum dragons: Rectangular graphs

Figure 12 shows results for quantum dragons based on a 2D rectangular graph with $\ell = 30$ and $m = 20$. The intra-slice nn hopping strengths were chosen completely at random, such that 50% of the bonds were cut and the remaining bond strengths were chosen independently, uniformly at random with $t_{i,j;i+1,j} \in [0.2, 1.8]$. The on site energies were chosen for the device to be a quantum dragon from Eq. (20) with a uniform \vec{v}_{Dragon} . The nnn inter-slice hopping strengths were chosen randomly such that 20% of the nnn bonds were present with $t_{i,j;i\pm 1,j+1} \in [0.1, 0.4]$ and the nn inter-slice hopping strengths chosen from Eq. (14) to make the device a quantum dragon. The disorder hence has only local correlations, but the device shows order amidst disorder. Figure 12(A) shows an example of such a quantum dragon nanodevice, while another view of the underlying graph is Fig. 12(B). Figure 12(C) shows the average transmission over 10^3 different strengths δ of uncorrelated on site disorder chosen from a Gaussian distribution of mean zero and width unity uniformly and then multiplied by δ . The four values of δ are 0.0 (light green, quantum dragon value), 0.08 (red), 0.16 (black), and 0.24 (blue). Each energy point plotted was run for 50 different quantum dragon nanodevices constructed with the type

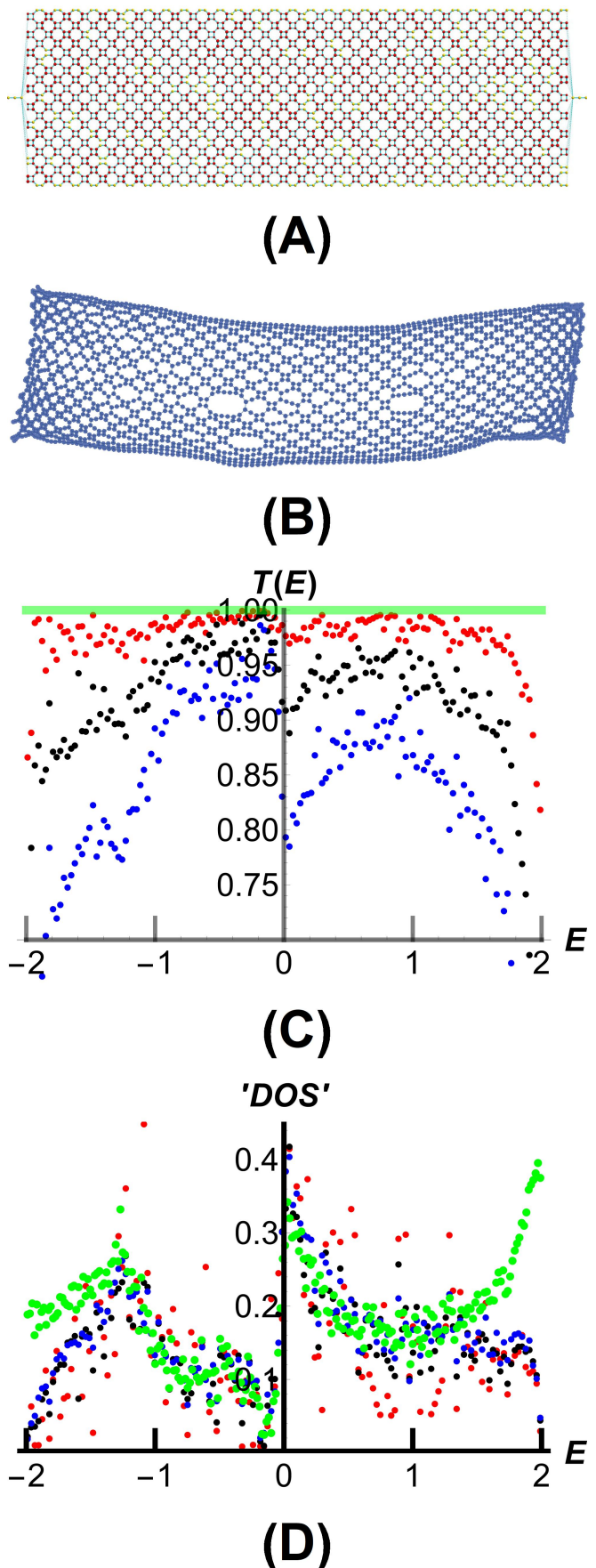


FIG. 11. A strongly disordered $\ell = 120$ and $m = 20$ nanoribbon based on a square-octagonal graph. See text Sec. VII.A for full description.

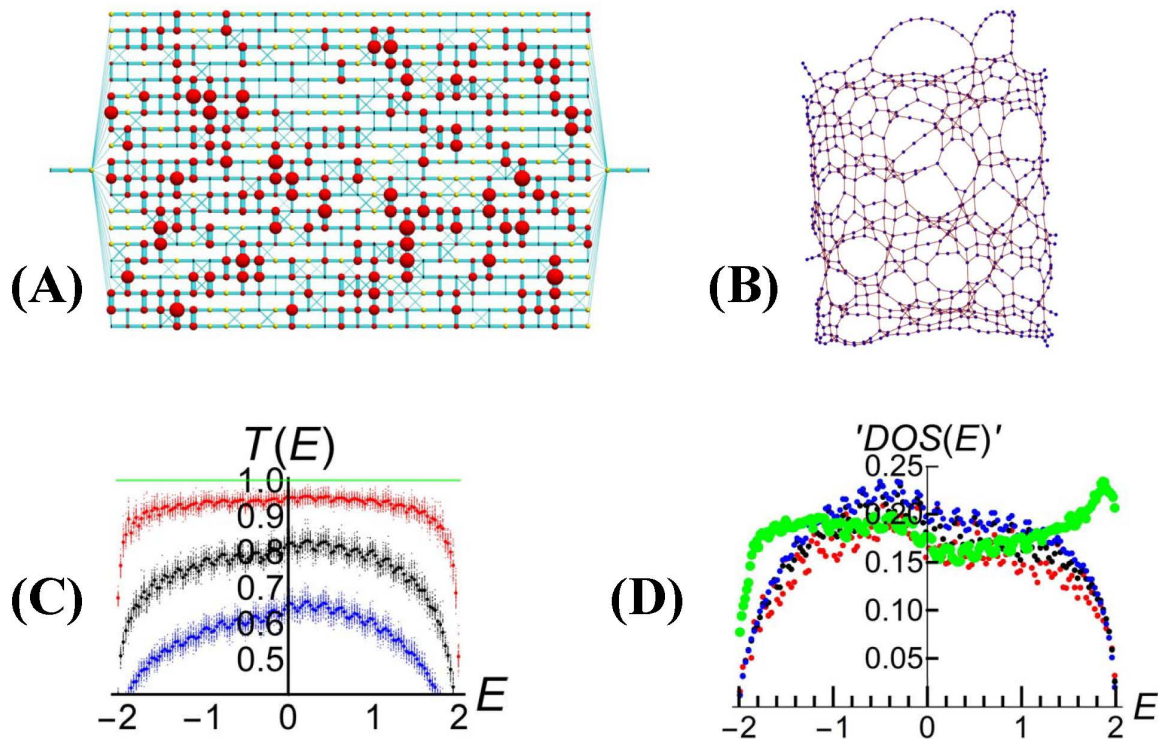


FIG. 12. Strongly disordered $\ell = 30$ and $m = 20$ nanoribbons based on 2D rectangular graphs. See text Sec. VII.B for full description.

of disorder described above and all 50 are plotted, together with their average (larger symbol size). The quantum dragon result, found for all 50 nanodevices, $\delta = 0$ is shown in light green with $\mathcal{T}(E) = 1$. Figure 12(D) shows the same finite δ values with the same color codes for the

average transmissions in Figure 12(C), scaled according to Eq. (18). The dark green points show the result for the DOS for all 50 device Hamiltonians, with a box counting using $\delta E = 0.15$. The agreement, with no adjustable parameters, is very good, except near the band edges at $E = \pm 2$.

VIII. ORDER AMIDST DISORDER: 3D GRAPHS

It is possible to also have 2D intra-slice graphs with strong locally-correlated disorder for each slice, giving a 3D overall graph after including the inter-slice bonds, and still have order amidst disorder and $\mathcal{T}(E) = 1$. For a given \vec{v}_{Dragon} with all positive elements, and indexing the intra-slice atoms by i (even though the intra-slice graph has m atoms arranged on a 2D graph) for any random choice of intra-slice bonds a quantum dragon nanodevice needs to have all on site energies satisfy Eq. (20). Hence one has also in 3D atypical disorder, but only locally correlated disorder, that allows for nanodevices exhibiting order amidst disorder.

An example for a uniform \vec{v}_{Dragon} is shown in Fig-

ure 13 for $\ell = 60$ and $m = 120$. The left $\ell/2$ slices have a 2D square graph (Fig. 13(A)) and right $\ell/2$ slices have a 2D triangular graph (Fig. 13(B)). In the figure we have chosen the inter-slice hopping matrices to all be $\mathbf{B}_{i,j;i,j+1} = -\mathbf{I}$. Each slice was considered to be divided into two regions. The intra-slice bonds were chosen from three distributions, depending on which region the atoms of the bonds belonged to, or if they were bonds between the two regions. We restricted ourselves to nn bonds, but had $\ell/2$ slices with a 2D square graph (a maximum of 4 nn intra-slice bonds per atom) and $\ell/2$ slices with a 2D triangular graph (a maximum of 6 nn intra-slice bonds per atom). In region #1 corresponding to black dots (#2 red dots) the nn intra-slice bond strengths were chosen uniformly from the distribution $[0, 0.5]$ ($[0.5, 1]$). Intra-slice nn bonds joining atoms from the two differ-

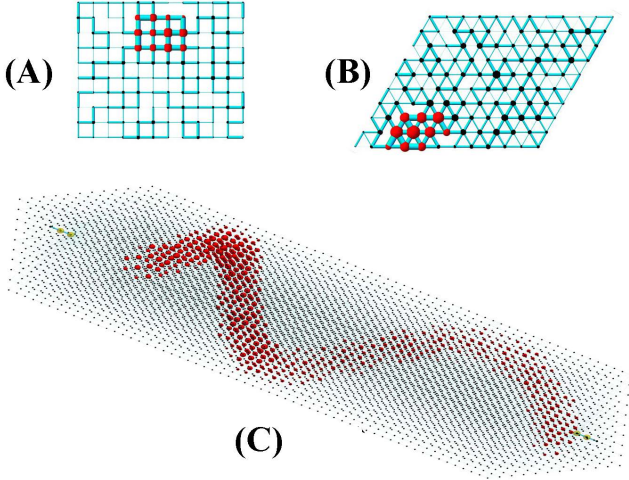


FIG. 13. Strongly disordered 3D structure with $\ell = 60$ and $m = 120$ based on each 2D slice being 10×12 . The radii of the two colors of spheres (red and black) are proportional to the on site energies, but are for regions with different distributions of randomly choosing the m intra-slice bond strengths. All bonds are shown as cyan cylinders, with radii proportional to the hopping strength. (A) Shows a 2D rectangular graph based slice. (B) Shows a 2D triangular graph based slice. The entire device is shown in (C) with $\ell/2$ 2D rectangular (left end of device) and $\ell/2$ 2D triangular (right end of device) intra-slice sub-graph slices. See text in Sec. VIII for a full description.

ent regions were chosen with a 50% chance to be zero and a 50% chance to have the strength 0.5. The on site energies were chosen to satisfy Eq. (20), so the nanodevice is a quantum dragon. Figure 13(A) shows one slice where the underlying 2D graph is a rectangular graph with free boundary conditions. Figure 13(B) shows one slice where the underlying 2D graph is a triangular graph with free boundary conditions. The strongly disordered quantum dragon nanodevice is shown in Figure 13(C). The device has $\mathcal{T}(E) = 1$ and exhibits order amidst disorder since the LDOS $_{i,j}$ is the same for every site.

IX. ORDER AMIDST DISORDER: 2D+3D COMBINATION GRAPHS

In Sec. VIII the method to combine different D-dimensional graphs with the same embedding dimension D to form a quantum dragon based on a D+1 dimensional graph was presented. It is also possible to combine intra-slice graphs with different embedding dimensions to obtain a combination graph for a quantum dragon nanodevice. In this section two examples are presented, one for fixed m and one for varying m .

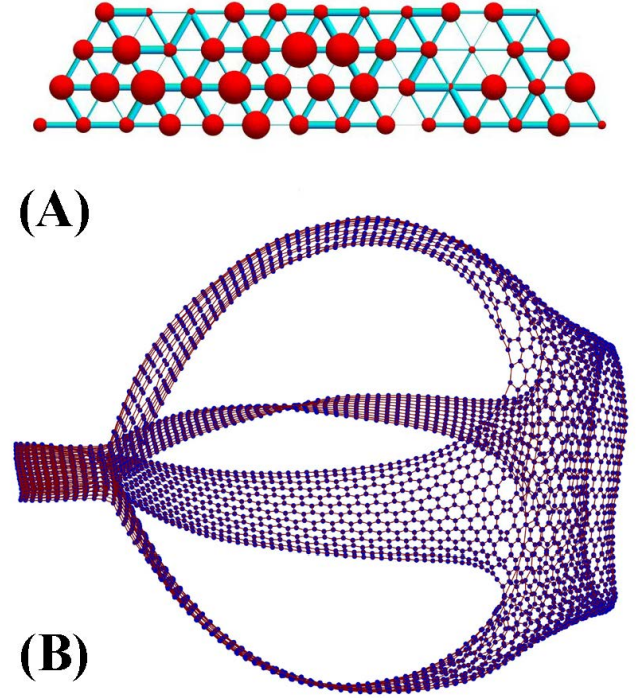


FIG. 14. A combination 2D+3D quantum dragon nanodevice with $\ell = 82$ and $m = 50$. (A) Shows a single slice of the 3D hexagonal graph portion of the nanodevice. The 3D sub-graph has 12 slices. (B) Shows the entire device, with the 3D sub-graph to the left. See Sec. IX.A for further information.

A. 2D+3D graphs: Fixed m

An example of a 2D+3D quantum dragon device is shown in Fig. 14(B), with $m = 50$ and $\ell = 82 = \ell_{3D} + \ell_{\text{ribbons}} + \ell_{\text{tube}}$. For convenience all inter-slice bonds were set to have $t_{i,j;i,j+1} = 1$, and the elements of \vec{v}_{Dragon} were chosen to all be equal to $m^{-1/2}$.

The 3D sub-graph is composed of $\ell_{3D} = 12$ slices of a 2D triangular graph composed of 4 layers with $m = 50 = m_1 + m_2 + m_3 + m_4$ with m_k atoms in layer k . The graph uses $m_1 = 11$ and $m_{k+1} = m_k + 1$. The intra-slice bonds for the 2D triangular sub-graphs were chosen at random with $t_{i,j;i',j} \in [0, 1]$. If an atom had $K_{i,j}$ intra-slice bonds labeled by α with values $t_{i,j;i+\alpha,j}$, the on site energies were chosen to satisfy

$$\epsilon_{i,j} = \sum_{\alpha=1}^{K_{i,j}} t_{i,j;i+\alpha,j}. \quad (22)$$

One of the ℓ_{3D} slices of the device in Fig. 14(B) is shown in Fig. 14(A). The radii of the cyan cylinders (red spheres) are proportional to the tight binding parameter values for the intra-slice hopping terms $t_{i,j;i+\alpha,j}$

(on site energies $\epsilon_{i,j}$). The 3D hexagonal sub-graph with $\ell_{3D} = 12$ is on the left in Fig. 14(B).

The middle sub-graphs are composed of ribbons, here $\ell_{\text{ribbons}} = 50$, with the same widths m_k as in the four layers of the 3D sub-graph. The intra-slice bonds present in the 2D graph of the ribbons were randomly chosen to have strength $t_{i,j;i+1,j} \in [0.98, 1.02]$, and the on site energies satisfy Eq. (22). If an atom has zero intra-slice bonds its on site energy is zero. The ribbon with $m_1 = 11$ is a 2D rectangular graph, and is given a half-twist before connecting to the right-most sub-graph. The ribbon with $m_2 = 12$ is a 2D square-octagonal graph, and is given a half-twist before connecting to the right-most sub-graph. The ribbon with $m_3 = 13$ is a zigzag 2D hexagonal nanoribbon. The ribbon with $m_4 = 14$ is a 2D hexagonal graph, with the ends a zigzag ribbon while in the middle the ribbon is stitched into a structure isomorphic to that of an armchair SWCNT.

The right-most sub-graph in Fig. 14(B) has $\ell_{\text{tube}} = 20$ slices, and the graph is isomorphic to an armchair SWCNT. The intra-slice hopping terms were randomly chosen to satisfy $t_{i,j;i+1,j} \in [0.9, 1.1]$, and the on site energies were chosen to satisfy Eq. (22).

From the paragraphs describing the makeup of the graph and tight binding parameters in Fig. 14 the amount of disorder is evident. Furthermore, all intra-slice hopping parameters were chosen randomly, while the disorder for the on site energies are only *locally correlated* since they satisfy Eq. (22). Nevertheless, the nanodevice shown in Fig. 14 is a quantum dragon since $\mathcal{T}(E) = 1$ for all $-2 < E < 2$, and for any energy every atom has the same value for $\text{LDOS}_{i,j}$ (not shown) so the device shows order amidst disorder.

B. 2D+3D graphs: Varying m

It is also possible to build quantum dragons from 2D and 3D sub-graphs with varying numbers of atoms in each slice. One example is shown in Fig. 15, with $\ell = 86$ slices. The device is composed of four different regions with the number of atoms in a slice in region k given by m_k and the number of slices in that region ℓ_k . The total number of atoms in Fig. 15 is $3456 = \sum_{k=1}^4 m_k \ell_k$. In region k the intra-slice Hamiltonian \mathbf{A}_j and the inter-slice Hamiltonians $\mathbf{B}_{j,j+1}$, defined in Eq. (5), are of size $m_k \times m_k$. For simplicity we take the common eigenvector in region k to be $\vec{v}_{\text{Dragon}}^{(k)} = 1/\sqrt{m_k}$ and the $\mathbf{B}_{j,j+1}$ to be the negative of the $m_k \times m_k$ identity matrix.

The four regions in Fig. 15, from left to right, are

1. Zigzag 2D hexagonal graph; $m_1 = 18$ and $\ell_1 = 20$;
2. 3D simple cubic 2-layer graph; $m_2 = 36$ and $\ell_2 = 18$; each layer has 18 atoms in every slice;

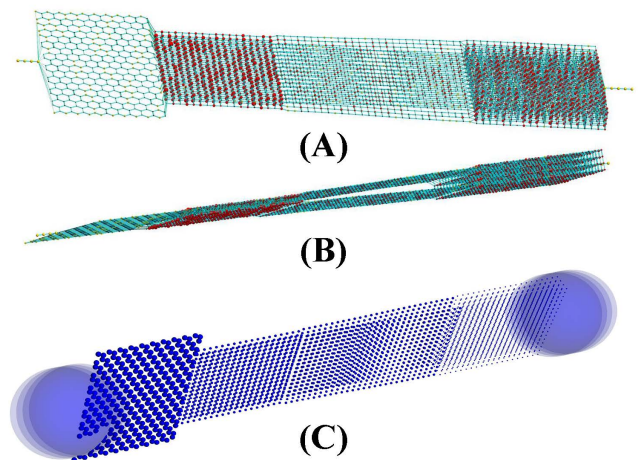


FIG. 15. A combination 2D+3D quantum dragon nanodevice with $\ell = 86$ and varying m with four different regions of the nanodevice. The nanodevice has 3456 atoms. (A) and (B) show two perspectives of the nanodevice. (C) shows the $\text{LDOS}_{i,j}(E)$ at $E = 1$. See Sec. IX.B for complete information.

3. Two ribbons formed by 2D square graphs; $m_3 = 36$ and $\ell_3 = 28$; each ribbon has 18 atoms in every slice;
4. 3D simple cubic 4-layer graph; $m_4 = 72$ and $\ell_4 = 20$; each layer has 18 atoms in every slice.

All intra-slice hopping terms were chosen so 20% of the bonds were missing, with other intra-slice hopping terms chosen uniformly at randomly with $t_{i,j;i+\alpha,j} \in [0.5, 1.5]$. The on site energies were then assigned as in Eq. (22), with the radii of the red spheres proportional to $\epsilon_{i,j}$. Note the 3D regions have typically larger on site energies because they typically have a larger coordination number than the 2D regions. The first region, on the left in Fig. 15, has the lead end atom connected to each of the m_1 atoms in slice $j = 1$ with hopping of strength $1/\sqrt{m_1}$. The fourth region, on the right in Fig. 15, has the lead end atom connected to each of the m_4 atoms in slice $j = \ell$ with hopping of strength $1/\sqrt{m_4}$.

The coupling between the regions k and $k + 1$ is more complicated because the inter-slice matrices are not square. Consider connecting the 2D ribbon in region 1 to the 2-layer 3D graph in region 2, then since $m_2 = 2m_1 = 36$ the inter-slice hopping Hamiltonian $\mathbf{B}_{\ell_1,\ell_1+1}$ has dimensions 18×36 . It is easy to understand the required form of a proper connection by using a singular-value-decomposition (SVD) of $\mathbf{B}_{\ell_1,\ell_1+1}$. Require the SVD have a singular value $\sigma_{-1} = -1$ associated with the dragon vectors in the two regions, hence the two conditions are

$$\begin{aligned} \mathbf{B}_{\ell_1,\ell_1+1} \vec{v}_{\text{Dragon}}^{(2)} &= \sigma_{-1} \vec{v}_{\text{Dragon}}^{(1)} \\ \text{and} & \\ \mathbf{B}_{\ell_1,\ell_1+1}^\dagger \vec{v}_{\text{Dragon}}^{(1)} &= \sigma_{-1} \vec{v}_{\text{Dragon}}^{(2)}. \end{aligned} \quad (23)$$

In order to make a simple and physical connection we use the method in Ref. [22], which uses the generalizations of the Kronecker matrix product and notation of Ref. [53], and choose

$$\mathbf{B}_{\ell_1, \ell_1+1} = -\frac{1}{\sqrt{2}} \left\{ \mathbf{J}_{18 \times 2} \quad \mathbf{I}_{18 \times 18} \right\} \quad (24)$$

with the identity matrix \mathbf{I} and matrix \mathbf{J} with all values unity, both of the shown dimensions. Here in region 2 the atoms in the top layer are numbered 1-18, the bottom layer numbered 19-36, and there is a possible intra-slice hopping term between atoms indexed as $i, 21$ and $i + 18, 21$. In words, the end atom from region 1 is connected with hopping strengths $1/\sqrt{2}$ to the two associated end atoms in the top and bottom layer in region 2. We use the same type of connection between region 3 and region 4, connecting the top ribbon to the top two layers and the bottom ribbon to the bottom two layers.

Even though the device has significant disorder, every slice is different from every other slice, and the sub-graphs in the four regions are different and have a different value for m_k . Nevertheless, the nanodevice in Fig. 15 is a quantum dragon since it has $\mathcal{T}(E) = 1$ for $-2 < E < 2$. Furthermore, it shows order amidst disorder in the LDOS $_{i,j}(E)$ for any $-2 < E < 2$, as seen in Fig. 15(C) for the energy $E = 1$. Here the radii of the blue spheres are proportional to LDOS $_{i,j}$. Every atom in each region has the same value for the LDOS, and furthermore the sum over all atoms within a slice has the same value for $\sum_{i=1}^{m_k} \text{LDOS}_{i,j}$. The lead end atoms (the largest spheres) have a LDOS which is m_k times larger than the individual LDOS $_{i,j}$ of the atoms in region k . These findings agree with the predictions for the LDOS of Eq. (13) with the substitution $m \rightarrow m_j$ in each slice (compare Eq. (D2)).

X. DISCUSSION AND CONCLUSIONS

We believe this paper addresses long-standing problems and has implications in a number of fields, from understanding disordered quantum systems to potential advances in electronics based on physical nanodevices. The fundamental conclusion is that even with **extensive** disorder, and with only **local** correlations in disorder, **quantum dragon nanodevices** exist. We have shown that quantum dragon nanodevices exhibit **order amidst disorder**.

We have studied the coherent electron transport in model systems, with the system comprised of an underlying graph and an associated single-band tight binding Hamiltonian as in Eq. (4). The graph and/or the Hamiltonian may have extensive disorder, as long as there is proper local correlations so one has a quantum dragon nanosystem.

The traditional methods of approaching and analyzing disordered quantum systems are very different from

our approach that finds **order amidst disorder** and quantum dragons. Furthermore, there are wide classes of different nanodevices with atypical disorder which are quantum dragons. The Supplemental Material [54] is designed to allow the user to experience much more of the zoo of quantum dragons. The Supplemental Material includes ten `.cdf` files [39] allowing for 3D manipulations of some of the figures. More importantly, the Supplemental Material also contains four `.cdf` programs in which the user can change parameters and create their own quantum dragon nanodevices and nanodevices that are nearly quantum dragons. Utilizing the Supplemental Material `.cdf` files, and the related `.pdf` as a ‘user manual’, should allow students to gain a much better understanding of our unique approach to disordered quantum nanodevices.

A. Analysis of disordered quantum models

Ordered systems are analyzed theoretically by exploiting translational invariance. For quantum systems this typically involves using Bloch wavefunctions and a band structure analysis. Hence most textbooks on solid state physics start with crystal structures and exploit the crystal structure to obtain electron transport properties [55–57]. If there is translational invariance one then has a Hamiltonian that can be written as a sum over Fourier coefficients, and assigns the Fourier coefficient with wavevector \vec{k} to a quasi-particle electron with that wavevector. For systems with weak disorder, disordered models are taken to be due to perturbations about the ordered crystalline structure.

However, consider taking a Fourier transform of a disordered quantum dragon. Because of the extensive nature of the disorder in the model Hamiltonians and graphs we study, these traditional theoretical tools cannot be applied. At least for the case of general \vec{v}_{Dragon} the Fourier coefficients will not correspond to a useful quasi-particle description.

Rather than using translational invariance to analyze coherent electron transport, we have generalized the mapping method [22], as detailed in Sec. III and sketched in Fig. 1. This allows one to calculate the electron transmission $\mathcal{T}(E)$ when a nanosystem is connected to two semi-infinite uniform leads. This method does not always work, in fact it is only for configurations with atypical disorder that the mapping method is useful. In some instances where the mapping method works, as sketched in Fig. 1, the mapping yields a uniform 1D wire and the nanodevice is a quantum dragon with $\mathcal{T}(E) = 1$ for all electron energies E in some finite range. We have shown the quantum dragons exhibit **order amidst disorder**, for example the LDOS $_{i,j}(E)$ evince translational invariance.

B. Carbon-based nanodevices

One conclusion is for nanomaterials and nanodevices based on 2D hexagonal graphs, as in Sec. VI. Consider first materials based only on carbon atoms at the graph vertices. The tight binding model has been used in theoretical investigations [58] to understand the novel electrical properties of graphene [24, 59] and SWCNTs [60, 61]. As in Table I, currently known SWCNTs with $\mathcal{T}(E) = 1$ undergo ballistic electron propagation due to their ordered structure. For example, armchair SWCNTs are metallic and allow very high current densities (over 10^9 A/cm² and hence more than 10^3 times that of copper) far above room temperature [62]. The coherent electron transport in the armchair SWCNT, which exhibits ballistic electron transmission, can be analyzed using the mapping method [22]. Therefore, the armchair SWCNT can be considered to be a quantum dragon with zero disorder. The common folklore is that adding any amount and type of disorder destroys the $\mathcal{T}(E) = 1$ property due to the scattering of the coherent electrons by the disorder. The disorder definitely causes scattering of the electrons. However, we have shown this does not mean the property $\mathcal{T}(E) = 1$ has to be destroyed! We have explicitly demonstrated the nanomaterial remains a quantum dragon, and hence has $\mathcal{T}(E) = 1$ and shows **order amidst disorder**, when the underlying graph and Hamiltonian undergo proper operations of:

- printing;
- cutting (or unzipping);
- sewing (or zipping);
- twisting;
- braiding;
- moving, adding and/or removing bonds;
- combinations of the above.

If these operations are done improperly, the nanodevice no longer has $\mathcal{T}(E) = 1$.

Carbon-based nanosystems synthesized along the operation of cutting (or unzipping) have a relatively long experimental history. The unzipping is one way to produce uniform GNRs by cutting a CNT, as seen experimentally in Refs. [63–71]. These experiments often also report partially-open CNTs, as for example depicted in Fig. 7. Furthermore, partially unzipped carbon nanotubes have been studied for their potential use to enhance the strength of the composite interface when used as part of a composite [72, 73] and as potential electrode material [74].

A 2009 paper investigated partially cut (partially unzipped) CNTs, and concluded *... partially open CNTs may offer unique opportunities for the future development of nanoscale electronics and spintronics*. They were considering nanodevices as in Fig. 7 We agree with that

assessment, but believe with quantum dragon nanodevices the possibility of applications to nanoelectronics and nano-spintronics is even more pronounced, since now rather than just proper cutting there is the host of other proper operations which can be made and keep the device a quantum dragon. We have not studied in this article the possibilities of adding external transverse electric fields or magnetic fields. However, one can expect the Fig. 8 will demonstrate differences to the non-twisted case with the non-twisted case expected to exhibit magnetic flux quantization. The effect of external electric and magnetic fields on braided quantum dragons as in Fig. 9 and on tatty quantum dragons as in Fig. 10 is an open topic.

C. Non-carbon-based nanodevices

Quantum dragons should have drastic experimental applications to nanosystems and nanodevices beyond those based on carbon. For example, even in 2013 an experimental method to unzip Boron Nitride Nanotubes (BNNTs) to form Boron Nitride Nanoribbons (BNNRs) was published [75]. For most nanodevice with more than one type of atom on a graph the analysis of this paper needs to be generalized to leads which have more than one atom in the lead unit cell. This generalization has already been accomplished for quantum dragon nanodevices that had randomness correlated across the device [22, 23]. Therefore, there should be no problems with generalizing to quantum dragons with only locally correlated randomness.

D. Extended states in $D > 1$

One conclusion addresses a long-standing open problem in mathematical physics. The problem [10] is to:

- *Establish the existence (in some energy range) of extended eigenstates, or continuous spectrum, for linear operators with **extensive** disorder. A prototypical example is the discrete Schrödinger operator with random potential.*

We have studied the electron transport in the discrete Schrödinger operator, namely in the tight-binding model in Eq. (4). Because the quantum dragons have electron transmission $\mathcal{T}(E) = 1$ in the energy range $-2 < E < 2$, there must be at least one extended state to allow this transmission. The extended state manifests itself not in the physical basis where one writes the Hamiltonian as operators on the sites and bonds of a graph in D dimensions (in graph theory the sites are called vertices and the bonds are called edges [1]). Rather the extended state manifests itself in the ‘rotated’ or ‘mapped’ [22] basis as sketched in Fig. 1. The disorder we study is **extensive**, in that for example in Fig. 15 we could choose the intra-slice hopping terms $t_{i,j,i',j}$ from any distribution,

and still be able to satisfy the general constraint imposed by Eq. (20) for assigning the on site energies $\epsilon_{i,j}$. Eq. (20) imposes only a **local constraint** on the disorder. In 1D the presence of any (locally correlated) disorder leads to Anderson localization, and hence no extended states. We therefore postulate the following theorem:

Theorem: In any dimension $D > 1$ for the tight binding Hamiltonian there exists atypical, extensive, locally-correlated disorder systems which have at least one extended state and have electron transmission equal to unity for some energy range.

We have proven this theorem by explicit construction in 2D and 3D. The generalization to graphs with higher embedding dimensions is straightforward, as the method given by the local constraint of Eq. (20) does not depend on the embedding dimension and can be generalized to any coordination number. In fact, as the coordination number K increases, by the central limit theorem the on site energy that satisfies Eq. (20) will approach its average value. In other words, using braces $\langle \dots \rangle$ to denote the average value, one has

$$\langle \epsilon_{i,j} \rangle \longrightarrow K \langle t_{i,j;i',j} \rangle. \quad (25)$$

Furthermore, the width of the distribution of $\epsilon_{i,j}$ becomes narrower as K becomes larger. Hence although in 2D quantum dragons are atypical random configurations, in graphs with large K one expects the typical random configuration to either be or to be near a quantum dragon.

E. Nearly quantum dragon nanodevice circuits

No disordered quantum dragon nanodevice is expected to be a perfect quantum dragon, with $\mathcal{T}(E) = 1$ for a range of energies, due to uncorrelated disorder, edge effects for stable nanodevices, and/or operation at finite temperature. We have derived and demonstrated two scaling regimes for nanodevice which are very close to quantum dragons. Extremely close to a quantum dragon nanosystem, we find a universal scaling, Eq. (E11), that does not depend on any device parameters other than ℓ , m , the energy of the incoming electron, and variance δ^2 of the uncorrelated site disorder added to the quantum dragon nanosystem. For larger, but still small, added uncorrelated site disorder our scaling of Eq. (18) gives predictions for the average transmission $\mathcal{T}_{\text{ave}}(E)$ for an energy E of the incoming electron. The prediction only depends on the length L along the direction of current flow, δ^2 , E , and the density of states per atom $\text{DOS}(E)$. In both scaling cases the expected transmission at any energy is very close to unity. Therefore, it is very reasonable to assume quantum dragon nanodevices can be synthesized, constructed, measured, and utilized as parts of electronic, opto-electronic, or spintronic circuitry. For example, just as ballistic diodes and transistors utilize

the $\mathcal{T}(E) \approx 1$ property for ballistic electron propagation, quantum dragon diodes and transistors could utilize the $\mathcal{T}(E) \approx 1$ property.

The measurement, understanding, and utilization of ballistic electron propagation is over a hundred years old. For example, it gives the current-voltage characteristics of vacuum tubes, where it is known as the Child-Langmuir law [76, 77]. Carbon based nanotubes have been utilized as quantum wires [15] and made into transistors, including field-effect transistors (FETs) [16–20]. More recently, exploiting the $\mathcal{T}(E) \approx 1$ property has more been used to build a ballistic rectifier fabricated in single-layer graphene sandwiched by boron nitride flakes, exhibiting a mobility of $\sim 2 \times 10^5 \text{ cm}^2/\text{V}\cdot\text{s}$ and a voltage responsivity of $2.3 \times 10^4 \text{ V/W}$ with these properties holding to room temperature [78]. The $\mathcal{T}(E) \approx 1$ property also has allowed ballistic diodes operating in the THz range [79], due to the way electrons with $\mathcal{T}(E) \approx 1$ and large $v(E)$ (as in Sec. V) interact with electromagnetic radiation. The $\mathcal{T}(E) \approx 1$ has also been used to design a ballistic deflection transistor [80] and very recently a room temperature diode based on a ratcheting technique [81].

Therefore we speculate that just as quasi-ballistic nanodevices can be built using the $\mathcal{T}(E) \approx 1$ property, quasi-quantum dragon nanodevices could be designed and built using the $\mathcal{T}(E) \approx 1$ property. One of the main obstacles of designing a quasi-ballistic device is that minor changes to the geometry or disorder causes strong scattering of the electrons and $\mathcal{T}(E)$ rapidly becomes small. We had demonstrated that quasi-quantum dragon devices can have allowed changes to the geometry (for example by cutting, twisting, and braiding) and **locally** to the disorder all while keeping the $\mathcal{T}(E) \approx 1$ property. These allowed local (in the Hamiltonian) and global (in the geometry and topology) changes can be incorporated into designs of nanodevices based on being nearly quantum dragons. We anticipate that now that we have predicted the $\mathcal{T}(E) = 1$ property for such nanosystems they can be made into excellent sensors for electromagnetic radiation and magnetic fields as well as into diodes and transistors.

F. Cloaking in coherent quantum systems

Quantum dragon nanosystems have $\mathcal{T}(E) = 1$ for a finite range of energies. They occur in any $D > 1$ for select graphs (ordered or disordered) and select quantum Hamiltonians, the system is the graph + the quantum Hamiltonian. Quantum dragon systems may be based either on physically motivated systems as in this paper or on more general systems [22].

In either case, quantum dragons exhibit what may be called **coherent quantum cloaking**. Assume the only way to investigate a black-box system with a nanodevice is to study the coherent electron transmission, i.e. measure $\mathcal{T}(E)$. From such a measurement one cannot

tell whether there is a uniform wire inside the black-box or one or more quantum dragon nanodevices. In other words, by adjusting properly the quantum Hamiltonian of a nanodevice the fact there is a nanodevice within the black-box is cloaked because all incoming electrons in a finite range of energies undergo complete electron transmission. This lack of reflection of the incoming coherent electrons means the nanodevice has been cloaked from this quantum measurement. The cloaking can be accomplished with proper modifications of the disordered graph and/or quantum Hamiltonian.

G. Quantum dragons in QIP and QC

The concept of quantum dragons, and the method of devising and analyzing them, may have applications in QIP (Quantum Information Processing) and QC (Quantum Computing).

One example are special-purpose quantum device which can simulate coherent transport, and have been used to also study quantum walks. Although most of the work has been done on 1D graphs (1 space and 1 time) [82, 83], recent work has also included 2D graphs (2 space and 1 time) [84]. Future generations of related quantum devices for simulation of quantum transport could be used to investigate quantum dragon systems, and systems that are near quantum dragons.

Gate-based QC proceeds by performing a series of M_{QC} unitary operators on an initial qubit state, and performs a measurement in the Cbit (classical bit) basis after the computation. The power of QC comes from the non-commutative property of the unitary operators. For N_{QC} qubits the operators are $2^{N_{\text{QC}}} \times 2^{N_{\text{QC}}}$. The existence of quantum dragons demonstrates interesting properties of quantum systems due to a set on non-commuting matrices having a common eigenvector. An open question is whether requiring all M_{QC} unitary operators to have one or more common eigenvectors leads to interesting algorithms and applications in QC and QIP.

ACKNOWLEDGMENTS

This material is based on research sponsored for M.A.N. by the Air Force Research Laboratory (AFRL) under agreement number FA8750-18-1-0096. The U.S. Government is authorized to reproduce and distribute reprints for Governmental purposes notwithstanding any copyright notation thereon. The views and conclusions contained herein are those of the authors and should not be interpreted as necessarily representing the official policies or endorsements, either expressed or implied, of the Air Force Research Laboratory (AFRL) or the U.S. Government. US patent pending, filing PCT/US15/00114. M.A.N. acknowledges funding as a Fulbright Distinguished Chair, and thanks the students, faculty, and staff of the Charles University Faculty of Mathematics

and Physics for their warm hospitality during which this collaboration was initiated. T.N. acknowledges support by the Czech Science Foundation via project No. 19-13525S, the Czech Ministry of Education, Youth and Sports via INTER-COST project LTC19045, and the National Science Centre (NCN, Poland) via Grant No. UMO-2017/27/B/ST3/01911.

Appendix A: Matrices with a common eigenvector

As in Ref. [22] and Sec. III, the most important ingredient for finding quantum dragons where every slice has m atoms is that all ℓ of the $m \times m$ intra-slice Hamiltonian \mathbf{A}_j and all $\ell - 1$ parts of the inter-slice submatrices $\mathbf{B}_{j,j+1}$ of Eq. (5) have a common eigenvector. This common eigenvector \vec{v}_{Dragon} is a length m normalized vector with no zero elements. Matrices with a single common eigenvector do not commute, but do form a group structure [85, 86]. As shown in Ref. [22] to obtain $\mathcal{T}(E)=1$ the connections between the leads and the first and last slice of the nanodevice are given by \vec{v}_{Dragon} as described in Sec. IV. This allows the mapping used in Ref. [22], which is the similarity transformation described in Sec. III. The remaining $m-1$ eigenvectors of each of the \mathbf{A}_j and $\mathbf{B}_{j,j+1}$ may depend on j , but are not important for the electron transmission since they are then disconnected from the leads, as sketched in Fig. 1.

Appendix B: 1D quantum wire

The 2D, 3D, or 2D/3D nanodevice is connected to thin 1D uniform semi-infinite leads. Furthermore, as sketched in Fig. 1 the quantum dragon nanodevice has a uniform quantum wire in the rotated basis of Hilbert space. It is this property that enables order amidst disorder in the disordered nanodevice after the similarity transformation. Therefore, the electron transmission of a uniform quantum wire is of extreme importance.

Let ϵ_{Lead} be the on site energy value for all lead atoms, and t_{Lead} be the hopping strength between nn pairs of atoms in the uniform wires. The right lead has the tight binding Hamiltonian

$$\mathcal{H}_{\text{R,Lead}} = \epsilon_{\text{Lead}} \sum_{j=j_0}^{\infty} c_j^\dagger c_j - t_{\text{Lead}} \sum_{j=j_0}^{\infty} \left(c_j^\dagger c_{j+1} + c_{j+1}^\dagger c_j \right) \quad (\text{B1})$$

with j_0 the index of the lead atom attached to the nanodevice.

Let a be the nn distance between lead atoms. A Bloch wavefunction analysis for the uniform wire gives the dispersion relation

$$E = -2t_{\text{Lead}} \cos(q_{\text{Lead}}a) \quad (\text{B2})$$

with electron wavevector in the leads q_{Lead} . The lead wires are uniform so they can be regarded as a short

circuit device, which has complete transmission,

$$\mathcal{T}(E) = 1 \quad \text{for all } -2t_{\text{Lead}} < E < 2t_{\text{Lead}}. \quad (\text{B3})$$

We choose the zero of energy to be $\epsilon_{\text{Lead}} = 0$. We also choose as our unit of energy the hopping strength $t_{\text{Lead}} = 1$. Hence we have set the zero of energy as well as the units of energy. There is a similar Hamiltonian for the left lead, again with $\epsilon_{\text{Lead}} = 0$ and $t_{\text{Lead}} = 1$.

Thus a uniform wire means complete transmission for all electron wavelengths which propagate in the leads, namely $2a \leq \lambda_{\text{Lead}} < \infty$. A transfer matrix method analysis actually shows there is complete transmission for $-2 \leq E \leq 2$ even in a non-uniform case as long as $|t_{\text{Lead}; j, j+1}|=1$ for each hopping term between nearest-neighbor atoms in the 1D wire, i.e. phases are allowed as they do not change the electron transmission from being $\mathcal{T}(E) = 1$.

Appendix C: Bond current calculations

We stress the way we calculate the transmission, as well as both the LDOS and the local currents, are by the usual NEGF formulas. Setting $a = 1$ for the distance between lead atoms, with

$$\xi = e^{-iq_{\text{Lead}}} = -\frac{E}{2} - i\frac{\sqrt{4-E^2}}{2} \quad (\text{C1})$$

the self energies of the left and right leads are then $\Sigma_L = -\xi^* \vec{L} \vec{L}^\dagger$, $\Sigma_R = -\xi^* \vec{R} \vec{R}^\dagger$ (see Sec. IV). The Green's function is given by Eq. (10). The transmission $\mathcal{T}(E)$ is then given by Eq. (9) with $\Gamma_L = \sqrt{4-E^2} \vec{L} \vec{L}^\dagger$ and $\Gamma_R = \sqrt{4-E^2} \vec{R} \vec{R}^\dagger$. For any size nanodevice and for any device Hamiltonian the calculations can in principle be performed, requiring only manipulations of $N \times N$ ma-

trices with $N = \sum_{j=1}^{\ell} m_j$. It is the precise form of the quantum dragon Hamiltonians which allow us to find $\mathcal{T}(E)=1$ for all $-2 < E < 2$ and order amidst disorder, even for arbitrarily large N values.

For the local currents one also introduces the lesser Green's function $\mathcal{G}^<$ in the conventional fashion [29, 30]. Define

$$\mathcal{G}^<(E) = \mathcal{G} \Sigma^< \mathcal{G}^\dagger, \quad (\text{C2})$$

with $\Sigma^<(E) = i[\Gamma_L(E)f(E - \mu_L) + \Gamma_R(E)f(E - \mu_R)]$, $f(E)$ being the Fermi-Dirac function and $\mu_{L,R}$ the chemical potentials of the two leads. For simplicity we further restrict ourselves to zero temperature. With this approximation, one has $\Sigma^< \approx i\Gamma_L$ for energies within the voltage bias window $\mu_L > E > \mu_R$. If there is a nonzero hopping term between sites at (i, j) and (i', j') , the local current density which flows in this bond is [29]

$$I_{i,j;i',j'}(E) = \mathcal{H}_{i,j;i',j'} \mathcal{G}_{i',j';i,j}^<(E) - \mathcal{H}_{i',j';i,j} \mathcal{G}_{i,j;i',j'}^<(E). \quad (\text{C3})$$

Since $\mathcal{G}^<(E)$ is a function of energy, the usual situation is that the bond currents are functions of the energy too. However, for quantum dragon nanodevices the bond currents are independent of energy for $-2 < E < 2$ (if in the bias window).

We checked our calculations by ensuring the same total current flowed from slice j to the next slice $j+1$ for all $1 \leq j \leq \ell - 1$. For the graphs presented, both the LDOS and the local bond currents are re-scaled for the entire device to enhance the visual representation.

Appendix D: Order amidst disorder: any \vec{v}_{Dragon}

It is possible to obtain order amidst disorder using any normalized \vec{v}_{Dragon} , as illustrated for a 2D hexagonal graph in Fig. 16. The important concept to find a quantum dragon is \vec{v}_{Dragon} must be an eigenvector with eigenvalue zero for every intra-slice Hamiltonian \mathbf{A}_j (for $j = 1, 2, \dots, \ell$) and be an eigenvector with eigenvalue -1 for every inter-slice submatrix $\mathbf{B}_{j,j+1}$ (for $j = 1, 2, \dots, \ell-1$) with the matrices as defined in Eq. (5). The connection between the left lead with atoms in slice $j = 1$ and the connection between the right lead with atoms in slice $j = \ell$ are both accomplished using \vec{v}_{Dragon} .

Figure 16 shows an example for $m = 16$ and $\ell = 32$, with only the first 18 slices shown. The length m vector \vec{v}_{Dragon} was formed by having elements randomly chosen in $[0.05, 0.250]$ and then normalized, with specific values shown in Fig. 16(A). As shown in Fig. 16(B) all intra-

slice bonds were independently chosen at random with $t_{i,j;i+1,j} \in [0, 1]$, except a cut was placed from $j \in [9, 19]$ by setting $t_{5,j;6,j} = 0$. In Fig. 16(B) the random intra-slice bonds are shown as maroon cylinders with radii proportional to $t_{i,j;i+1,j} \in [0, 1]$, on the left a cyan cylinder with radius unity is shown for reference. The on site energies are then assigned in a fashion similar to Eq. (8), but generalized for an arbitrary \vec{v}_{Dragon} as

$$\begin{pmatrix} \epsilon_{i,j} & -t_{i,j;i+1,j} \\ -t_{i,j;i+1,j}^* & \epsilon_{i+1,j} \end{pmatrix} \begin{pmatrix} v_{\text{Dragon},i} \\ v_{\text{Dragon},i+1} \end{pmatrix} = \begin{pmatrix} 0 \\ 0 \end{pmatrix} \quad (\text{D1})$$

with $v_{\text{Dragon},i}$ the i^{th} element of \vec{v}_{Dragon} . The one constraint is that every element must satisfy $v_{\text{Dragon},i} \neq 0$. For simplicity, in Fig. 16 all inter-slice bonds are set to unity, $t_{i,j;i,j+1} = 1$. These steps lead to the device with

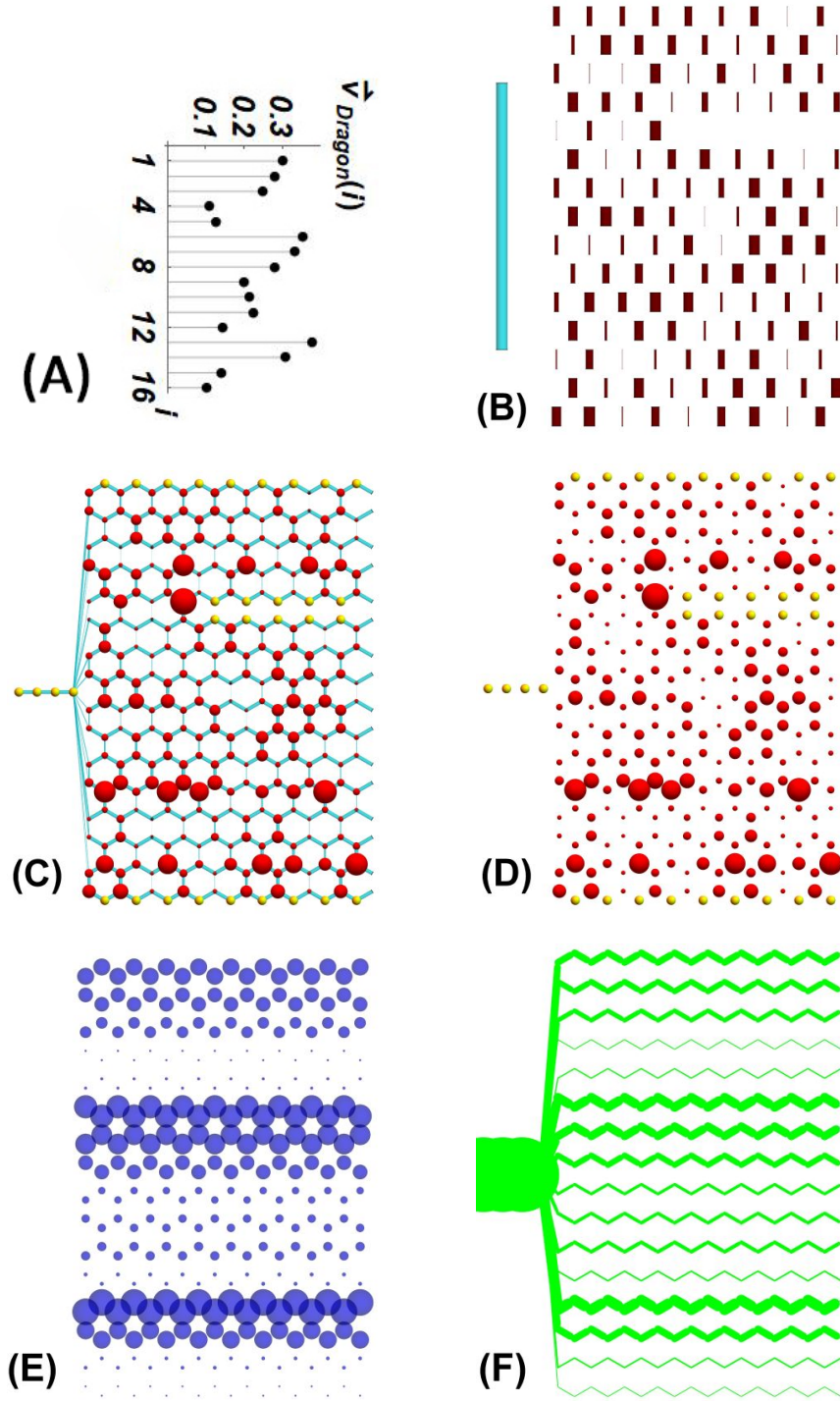


FIG. 16. Quantum dragon with arbitrary \vec{v}_{Dragon} . Parts (A)-(D) show the disorder, while order is seen in the LDOS $_{i,j}$ in (E) and the local bond currents in (F). See Appendix D for complete information.

the left-hand portion shown in Fig. 16(C), with bond strengths proportional to the radii of the cyan cylinders and the red sphere radii proportional to $\epsilon_{i,j}$ (except if $\epsilon_{i,j} = 0$ the atom is shown as a yellow sphere). In order to show the random nature of the disorder, Fig. 16(D) shows only the spheres associated with each on site en-

ergy.

From the Green's function $\mathcal{G}(E)$, the LDOS is calculated as in Eq. (12). The results from LDOS $_{i,j}(E)$ are shown in Fig. 16(E) with the values of LDOS $_{i,j}$ at $E = 1$ proportional to the radii of the blue spheres. We numer-

ically observed that for any energy we find

$$\text{LDOS}_{i,j}(E) = |v_{\text{Dragon},i}|^2 \frac{1}{\pi \sqrt{4 - E^2}}. \quad (\text{D2})$$

Note the LDOS of the lead atoms are not shown because they are much larger than the $\text{LDOS}_{i,j}$ within the device. Equation (D2), which generalizes the case of a uniform \vec{v}_{Dragon} of Eq. (13) which has every element equal to $1/\sqrt{m}$, is easy to prove. As in Fig. 1, in the rotated basis the LDOS of the uniform wire is uniform, and the unitary operator \mathbf{U}_N can be used to rotate back to the physical basis. Figure 16(E) demonstrates **order amidst disorder** since the $\text{LDOS}_{i,j}(E)$ values are independent of the slice index j for all energies.

The local currents are calculated from Eq. (C3), and depicted by green cylinders with radii proportional to $I_{i,j;i',j'}$ for $E = 1$ in Fig. 16(F). Figure 16(F) demonstrates order amidst disorder since all intra-slice local currents are zero ($I_{i,j;i+1,j} = 0$), and hence the incoming current splits into horizontal currents with $I_{i,j;i,j+1}$ independent of the slice number j for all i . The dependence of the local currents on the values of \vec{v}_{Dragon} gives that we could have ‘edge currents’ if we had the vector elements largest only at the ends of the vector. Alternatively, we could have currents that were only ‘middle currents’ if we chose the dependence of the \vec{v}_{Dragon} elements large only in the middle of the device.

Order amidst disorder is seen in Fig. 16, for any random \vec{v}_{Dragon} . If one looked at either the intra-slice bonds of Fig. 16(B) (every intra-slice bond is independent) or the on site energies in Fig. 16(D) the disorder is evident (every red sphere has a different radius). Nevertheless there is translational symmetry along the direction of current flow as seen both in the $\text{LDOS}_{i,j}(E)$ in Fig. 16(E)

and the local currents in Fig. 16(F).

Appendix E: NEGF and Dyson Series for small δ

We want to study the lowest perturbative correction to the quantum dragon transmission due to a very weak onsite disorder. We start from the trace formula Eq. (9) for the transmission coefficient in terms of the Green’s function (GF), reading

$$\mathcal{T}(E) = \text{Tr}[\mathbf{\Gamma}_L(E)\mathcal{G}(E)\mathbf{\Gamma}_R(E)\mathcal{G}^\dagger(E)] \quad (\text{E1})$$

with $\mathbf{\Gamma}_L(E) \equiv |L\rangle\gamma(E)\langle L|$ and $\mathbf{\Gamma}_R(E) \equiv |R\rangle\gamma(E)\langle R|$, where $\gamma(E) \equiv \sqrt{4 - E^2}$. The Green’s function Eq. (10) is basically just the resolvent of the system plus leads Hamiltonian projected by the partitioning method onto the system, i.e. the quantum dragon subspace. It is given by $\mathcal{G}(E) = (E - \mathcal{H} - \mathcal{V} - \mathbf{\Sigma}_L(E) - \mathbf{\Sigma}_R(E))^{-1}$, where the lead self-energies $\mathbf{\Sigma}_L(E) \equiv |L\rangle\sigma(E)\langle L|$ and $\mathbf{\Sigma}_R(E) \equiv |R\rangle\sigma(E)\langle R|$ with $\sigma(E) \equiv (E - i\sqrt{4 - E^2})/2$ and \mathcal{H} is the (unperturbed) quantum dragon Hamiltonian while $\mathcal{V} \equiv \sum_\alpha |\alpha\rangle v_\alpha \langle \alpha|$ is the perturbing scattering potential composed of site-uncorrelated disorder potentials satisfying the conditions (overbar denotes the impurity averaging) $\overline{v_\alpha} = 0$ and $\overline{v_\alpha v_\beta} = \delta^2 \delta_{\alpha\beta}$. Using the Dyson equation $\mathcal{G}^{-1}(E) = \mathcal{G}_0^{-1}(E) - \mathcal{V}$ with $\mathcal{G}_0(E)$ the unperturbed GF corresponding to the perfect quantum dragon solution and making its perturbative expansion up to the second order in the disorder $\mathcal{G}(E) \approx \mathcal{G}_0(E) + \mathcal{G}_0(E)\mathcal{V}\mathcal{G}_0(E) + \mathcal{G}_0(E)\mathcal{V}\mathcal{G}_0(E)\mathcal{V}\mathcal{G}_0(E)$ we arrive at the expansion of the transmission (E1) (keeping only the zeroth and second order terms since the first order term will cancel after the disorder averaging anyway)

$$\begin{aligned} \mathcal{T}(E) - 1 &\approx \text{Tr}[\mathbf{\Gamma}_L(E)\mathcal{G}_0(E)\mathbf{\Gamma}_R(E)\mathcal{G}_0^\dagger(E)] - 1 + \text{Tr}[\mathbf{\Gamma}_L(E)\mathcal{G}_0(E)\mathcal{V}\mathcal{G}_0(E)\mathbf{\Gamma}_R(E)\mathcal{G}_0^\dagger(E)\mathcal{V}\mathcal{G}_0^\dagger(E)] \\ &\quad + \text{Tr}[\mathbf{\Gamma}_L(E)\mathcal{G}_0(E)\mathcal{V}\mathcal{G}_0(E)\mathcal{V}\mathcal{G}_0(E)\mathbf{\Gamma}_R(E)\mathcal{G}_0^\dagger(E)] + \text{Tr}[\mathbf{\Gamma}_L(E)\mathcal{G}_0(E)\mathbf{\Gamma}_R(E)\mathcal{G}_0^\dagger(E)\mathcal{V}\mathcal{G}_0^\dagger(E)\mathcal{V}\mathcal{G}_0^\dagger(E)] \quad (\text{E2}) \\ &= \text{Tr}[\mathbf{\Gamma}_L(E)\mathcal{G}_0(E)\mathcal{V}\mathcal{G}_0(E)\mathbf{\Gamma}_R(E)\mathcal{G}_0^\dagger(E)\mathcal{V}\mathcal{G}_0^\dagger(E)] + 2\Re\{\text{Tr}[\mathbf{\Gamma}_L(E)\mathcal{G}_0(E)\mathcal{V}\mathcal{G}_0(E)\mathcal{V}\mathcal{G}_0(E)\mathbf{\Gamma}_R(E)\mathcal{G}_0^\dagger(E)]\}. \end{aligned}$$

Having done this, it’s time to use the specifics of quantum dragon solutions, in particular the unitary transform \mathbf{U}_N to the “uniform wire plus disconnected rest” basis. This will help us significantly simplify the general formula of Eq. (E2) above. In particular, we use the fact that the transformed coupling matrices have the following form $\mathbf{U}_N\mathbf{\Gamma}_L(E)\mathbf{U}_N^\dagger = \text{diag}[\gamma(E), 0, 0, \dots]$ and $\mathbf{U}_N\mathbf{\Gamma}_R(E)\mathbf{U}_N^\dagger = \text{diag}[0, \dots, \gamma(E), 0, 0, \dots]$ with the nonzero entry at the ℓ -th position. Furthermore, the transformed unperturbed, i.e. quantum dragon Green functions $\mathcal{G}_0(E)$, have a block-diagonal form reading

$$\mathbf{U}_N\mathcal{G}_0(E)\mathbf{U}_N^\dagger = \begin{pmatrix} \mathcal{G}_{\text{wire}}(E) & 0 \\ 0 & \mathcal{G}_{\text{rest}}(E) \end{pmatrix}$$

with the standard 1-D wire GF having matrix elements $\langle a|\mathcal{G}_{\text{wire}}(E)|b\rangle = -ie^{i\phi(E)}|a-b|/\gamma(E)$, with $\phi(E) \equiv \arccos(E/2)$. Plugging these transformed quantities into the first term on right hand side of the first line in Eq. (E2) we get

$$\begin{aligned} &\text{Tr}[\mathbf{\Gamma}_L(E)\mathcal{G}_0(E)\mathbf{\Gamma}_R(E)\mathcal{G}_0^\dagger(E)] \\ &= \gamma^2(E)\langle L|\mathcal{G}_0(E)|R\rangle\langle R|\mathcal{G}_0^\dagger(E)|L\rangle \quad (\text{E3}) \\ &= \gamma^2(E)\langle 1|\mathcal{G}_{\text{wire}}(E)|\ell\rangle\langle \ell|\mathcal{G}_{\text{wire}}^\dagger(E)|1\rangle \\ &= \gamma^2(E)|\langle 1|\mathcal{G}_{\text{wire}}(E)|\ell\rangle|^2 = 1 \end{aligned}$$

which is just the dragon solution as it must be.

Now, let’s consider the first term of the last line in Eq. (E2) and perform the disorder averaging. We get

the following expression for this term denoted as “ver” meaning *vertex correction*

$$\begin{aligned}\overline{\delta\mathcal{T}_{\text{ver}}} &= \text{Tr}[\mathbf{\Gamma}_L(E)\mathcal{G}_0(E)\mathcal{V}\overline{\mathcal{G}_0(E)\mathbf{\Gamma}_R(E)\mathcal{G}_0^\dagger(E)\mathcal{V}\mathcal{G}_0^\dagger(E)}] \\ &= \delta^2 \sum_\alpha \text{Tr}[\mathbf{\Gamma}_L(E)\mathcal{G}_0(E)|\alpha\rangle\langle\alpha|\mathcal{G}_0(E)\mathbf{\Gamma}_R(E)\mathcal{G}_0^\dagger(E)|\alpha\rangle\langle\alpha|\mathcal{G}_0^\dagger(E)] \\ &= \delta^2 \sum_\alpha \langle\alpha|\mathcal{G}_0(E)\mathbf{\Gamma}_R(E)\mathcal{G}_0^\dagger(E)|\alpha\rangle\langle\alpha|\mathcal{G}_0^\dagger(E)\mathbf{\Gamma}_L(E)\mathcal{G}_0(E)|\alpha\rangle.\end{aligned}\quad (\text{E4})$$

Here, we prove that the two constituents of the product $\langle\alpha|\mathcal{G}_0(E)\mathbf{\Gamma}_R(E)\mathcal{G}_0^\dagger(E)|\alpha\rangle$ and $\langle\alpha|\mathcal{G}_0(E)\mathbf{\Gamma}_L(E)\mathcal{G}_0^\dagger(E)|\alpha\rangle$ (complex-conjugated in Eq. (E4)) are actually independent of the site index α . Using the unitary transform \mathbf{U}_N we can rewrite the term $\langle\alpha|\mathcal{G}_0(E)\mathbf{\Gamma}_L(E)\mathcal{G}_0^\dagger(E)|\alpha\rangle$ (the other one follows analogously) as $\gamma(E)|\langle 1|\mathcal{G}_{\text{wire}}(E)\mathbf{U}_N|\alpha\rangle|^2$. Using Eq. (6) we have

$$\begin{aligned}\langle 1|\mathcal{G}_{\text{wire}}(E)\mathbf{U}_N|\alpha\rangle &= \sum_{\eta=1}^{\ell} \langle 1|\mathcal{G}_{\text{wire}}(E)|\eta\rangle(\mathbf{U}_N)_{\eta,\alpha} \\ &= \langle 1|\mathcal{G}_{\text{wire}}(E)|j\rangle/\sqrt{m}\end{aligned}\quad (\text{E5})$$

so that altogether

$$\langle\alpha|\mathcal{G}_0(E)\mathbf{\Gamma}_L(E)\mathcal{G}_0^\dagger(E)|\alpha\rangle = \frac{1}{m\gamma(E)}, \quad (\text{E6})$$

which is manifestly independent of the site index α . The

right term leads to the very same result so that we finally get

$$\begin{aligned}\overline{\delta\mathcal{T}_{\text{ver}}} &= \delta^2 \sum_\alpha \langle\alpha|\mathcal{G}_0(E)\mathbf{\Gamma}_R(E)\mathcal{G}_0^\dagger(E)|\alpha\rangle \\ &\quad \times \langle\alpha|\mathcal{G}_0^\dagger(E)\mathbf{\Gamma}_L(E)\mathcal{G}_0(E)|\alpha\rangle \\ &= \delta^2 \sum_\alpha \left(\frac{1}{m\gamma(E)}\right)^2 = \frac{\delta^2\ell}{m\gamma^2(E)}.\end{aligned}\quad (\text{E7})$$

Let’s now address the second term in the last line of Eq. (E2) corresponding to the renormalization of the single-particle GF — performing the disorder averaging we obtain (note that latin indices such as a, b denote the wire subspace spanned by sites $1 \dots \ell$ while the greek ones such as α are site indices in the original tight-binding basis for the whole dragon structure, i.e. $\alpha = \{i, j\}$ with $i = 1 \dots m, j = 1 \dots \ell$)

$$\begin{aligned}\overline{\delta\mathcal{T}_{\text{ren}}} &= 2\Re\{\text{Tr}[\mathbf{\Gamma}_L(E)\mathcal{G}_0(E)\overline{\mathcal{V}\mathcal{G}_0(E)\mathcal{V}\mathcal{G}_0(E)\mathbf{\Gamma}_R(E)\mathcal{G}_0^\dagger(E)}]\} \\ &= 2\Re\{\text{Tr}[\gamma(E)|L\rangle\langle L|\mathcal{G}_0(E)\mathcal{V}\overline{\mathcal{G}_0(E)\mathcal{V}\mathcal{G}_0(E)\gamma(E)|R\rangle\langle R|\mathcal{G}_0^\dagger(E)}]\} \\ &= 2\delta^2\Re\left\{\sum_\alpha \langle L|\mathcal{G}_0(E)|\alpha\rangle\langle\alpha|\mathcal{G}_0(E)|\alpha\rangle\langle\alpha|\mathcal{G}_0(E)|R\rangle\gamma^2(E)\langle R|\mathcal{G}_0^\dagger(E)|L\rangle\right\} \\ &= 2\delta^2\Re\left\{\frac{\sum_\alpha \langle L|\mathcal{G}_0(E)|\alpha\rangle\langle\alpha|\mathcal{G}_0(E)|\alpha\rangle\langle\alpha|\mathcal{G}_0(E)|R\rangle}{\langle L|\mathcal{G}_0(E)|R\rangle}\right\} \\ &= 2\delta^2\Re\left\{\mathcal{G}_0^{\text{loc}}(E)\frac{\sum_\alpha \langle L|\mathcal{G}_0(E)|\alpha\rangle\langle\alpha|\mathcal{G}_0(E)|R\rangle}{\langle L|\mathcal{G}_0(E)|R\rangle}\right\} \\ &= 2\delta^2\Re\left\{\mathcal{G}_0^{\text{loc}}(E)\frac{\langle 1|\mathcal{G}_{\text{wire}}^2(E)|\ell\rangle}{\langle 1|\mathcal{G}_{\text{wire}}(E)|\ell\rangle}\right\} = \frac{2\delta^2}{\gamma(E)}\Im\left\{\mathcal{G}_0^{\text{loc}}(E)\frac{\sum_{a=1}^{\ell} e^{i\phi(E)(\ell-a)}e^{i\phi(E)(a-1)}}{e^{i\phi(E)(\ell-1)}}\right\} \\ &= \frac{2\delta^2\ell}{\gamma(E)}\Im\left\{\mathcal{G}_0^{\text{loc}}(E)\right\}.\end{aligned}\quad (\text{E8})$$

We have used the unitary transmission condition (E3) when going from the second to the third line and the observed fact that (the imaginary part of) the site-local Green function $\langle\alpha|\mathcal{G}_0(E)|\alpha\rangle$ entering Eq. (12) is a site-independent function of energy denoted here by $\mathcal{G}_0^{\text{loc}}(E)$. Now, let’s evaluate this quantity

$$\begin{aligned}\Im\left\{\mathcal{G}_0^{\text{loc}}(E)\right\} &= \Im\langle\alpha|\mathcal{G}_0(E)|\alpha\rangle = \frac{1}{2i}\langle\alpha|\mathcal{G}_0(E) - \mathcal{G}_0^\dagger(E)|\alpha\rangle = -\frac{1}{2i}\langle\alpha|\mathcal{G}_0(E)[\mathcal{G}_0^{-1}(E) - (\mathcal{G}_0^\dagger(E))^{-1}]\mathcal{G}_0^\dagger(E)|\alpha\rangle \\ &= -\frac{1}{2}\langle\alpha|\mathcal{G}_0(E)[\mathbf{\Gamma}_L(E) + \mathbf{\Gamma}_R(E)]\mathcal{G}_0^\dagger(E)|\alpha\rangle = -\frac{1}{\gamma(E)m},\end{aligned}\quad (\text{E9})$$

where we have used Eq. (E6) in the last step. This finally leads to the expression

$$\overline{\delta\mathcal{T}_{\text{ren}}} = -\frac{2\delta^2\ell}{\gamma^2(E)m}, \quad (\text{E10})$$

and altogether we arrive at the final small δ universal

scaling law reading

$$\begin{aligned}\mathcal{T}_{\text{ave}}(E) &= 1 - \frac{\delta^2}{4-E^2} \frac{\ell}{m} \\ &\text{or} \\ [1 - \mathcal{T}_{\text{ave}}(E)] \frac{(4-E^2)m}{\ell\delta^2} &= 1.\end{aligned}\quad (\text{E11})$$

In Eq. (E11) it is important to keep in mind the range

of validity for the scaling. For example, although for large m one has $\mathcal{T}(E) \rightarrow 1$, this result is valid only for very small δ . The region of validity of Eq. (E11) is such that as m becomes larger one must have δ becoming smaller. For any given quantum dragon nanodevice (fixed graph and fixed Hamiltonian) as δ becomes larger, three regimes of scaling will be observed. First the universal behavior of Eq. (E11) will be valid. Then the scaling of Eq. (18) becomes valid, with scaling depending on E and $\text{DOS}(E)$. Finally when $\ell_{\mathcal{T}} \approx L$, i.e. when $\mathcal{T}(E) \approx \frac{1}{2}$, the well-studied regime of diffusive transport will be seen (Table I).

Furthermore, we have also explicitly evaluated the local density of states in Eq. (12), as reported in Eq. (13), as

$$\begin{aligned} \text{LDOS}_{i,j}(E) &\equiv -\frac{1}{\pi} \Im \langle \alpha | \mathcal{G}_0(E) | \alpha \rangle \\ &= \frac{1}{\pi m \sqrt{4-E^2}}. \end{aligned} \quad (\text{E12})$$

See Fig. 17 for a test of Eq. (E11). The data are for five types of nanodevices:

- **Green symbols:** Single-walled nanotubes with three values of (m, ℓ) .
 - With (m, ℓ) given by (12, 37):disks, (6, 37):squares, and (12, 18):triangles.
- **Magenta symbols:** 2D+3D device with constant m , as in Fig. 14 with two values of m .
 - With (m, ℓ) given by (18, 32):disks and (10, 32):squares.
- **Blue symbols:** 3D device with constant m , as in Figure 13.
 - With (m, ℓ) given by (18, 20):disks.
- **Red symbols:** 2D+3D nanodevice as in Fig. 15 with varying values of m in each slice. For a uniform \vec{v}_{Dragon} but with varying values of the number of atoms in the j^{th} slice, m_j , the scaling uses a value m_{Scale} for m in Eq. (E11), with m_{Scale} given by

$$\frac{1}{m_{\text{Scale}}} = \frac{1}{\ell} \sum_{j=1}^{\ell} \frac{1}{m_j}. \quad (\text{E13})$$

- Here $m\ell = N = 372$ given by the open disks.

- **Black symbols:** Linear chains with $m = 1$ and two values of ℓ .

- With (m, ℓ) given by (1, 37):disks, (1, 18):squares.
- For $m = 18$ at the smallest $\mathcal{T}_{\text{ave}}(E)$ values shown ten different averages, each using 10^4 configurations of uncorrelated site disorder, are shown.

In all cases in Fig. 17 the filled plotting symbols are for regular graphs and pure (not random) $\epsilon_{i,j}$ and $t_{i,j;i',j'}$, while the open plotting symbols are for corresponding graphs with 20% of the intra-slice bonds cut and the other intra-slice hopping terms $t_{i,j;i',j'} \in [0, 2]$. In all cases the dragon condition Eq. (22) is used to obtain the $\epsilon_{i,j}$ on site energy values. The averages are over 10^4 Gaussian-distributed uncorrelated values added to each dragon condition on site energy. The Gaussian distribution has mean zero and width unity, and is then multiplied by δ . The averages must be over a large number of disorder configurations, due to the narrow Fano resonance dips to $\mathcal{T}(E) = 0$ seen in Fig. 3(B). For all five nanodevices in Fig. 17, the same device (the same graph and the same Hamiltonian) are plotted. Only the 10^4 realizations of the disorder and the two energies, (A) for $E = 1$ and (B) for $E = -\sqrt{2}$, are different. With no adjustable parameters, in Fig. 17 we see for small δ excellent agreement with Eq. (E11) for all nanodevices. The only prediction we do not have is when for a particular type of quantum dragon the universal scaling breaks down as δ becomes larger. This is probably a complicated function of ℓ , m , $\text{DOS}(E)$, E , and perhaps the precise location of the disorder in the quantum dragon nanodevice. In Fig. 17(A) the energy $E = 1$ shown is near a minimum for the $\text{DOS}(E)$ for the single-walled nanotubes (green points). For a given quantum dragon nanodevice the universal scaling breaks down as δ increases at different values of δ , and hence at different values of $\mathcal{T}_{\text{ave}}(E)$, at different energies as seen most readily by comparing the SWNT (green) and 3D (blue) symbols in (A) and (B). We observed very similar behavior for all energies we tested in $-2 < E < 2$, with the only difference from Fig. 17 how large δ had to be before the universal scaling of Eq. (E11) broke down. This dependence of the scaling breakdown depending on E was also observed in the inset of Fig. 4 for a different quantum dragon nanodevice.

[1] G. Chartrand and P. Zhang, *A First Course in Graph Theory*, dover ed. (2012).
[2] P. W. Anderson, Phys. Rev. **109**, 1492 (1958).
[3] A. Lagendijk, B. van Tiggelen, and D. S. Wiersma, Physics Today **62**, 24 (2009).
[4] F. M. Izrailev and A. A. Krokhin, Phys. Rev. Lett. **82**,

4062 (1999).
[5] F. M. Izrailev, A. A. Krokhin, and N. M. Makarov, Phys. Rep. **512**, 125 (2012).
[6] S. Yu, X. Piao, J. Hong, and N. Park, Nature Commun. **6**, 8269 (2015).
[7] W. Choi, C. Yin, I. R. Hooper, W. L. Barnes, and

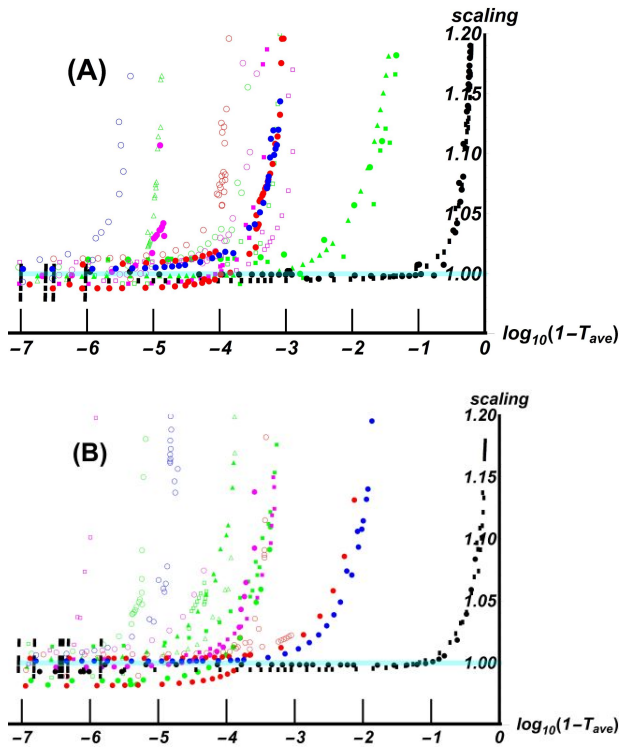


FIG. 17. A test of the small δ universal scaling of Eq. (E11), for five different types of nanodevices depicted by the five different colors. The energies shown are (A) $E = 1$ and (B) $E = -\sqrt{2}$. See Appendix E for complete information.

- J. Bertolotti, Phys. Rev. E **96**, 022122 (2017).
- [8] J. C. Flores, J. Phys. Condens. Matter **1**, 8471 (1989).
- [9] J. Bertolotti, S. Gottardo, D. S. Wiersma, M. Ghulinyan, and L. Pavesi, Phys. Rev. Lett. **94**, 113903 (2005).
- [10] M. Aizenman, “Extended states,” Princeton University, web.math.princeton.edu.
- [11] E. Abrahams, P. W. Anderson, D. C. Licciardello, and T. V. Ramakrishnan, Phys. Rev. Lett. **42**, 673 (1979).
- [12] R. Landauer, IBM J. Res. Dev. **1**, 223 (1957).
- [13] M. Büttiker, Y. Imry, R. Landauer, and S. Pinhas, Phys. Rev. B **31**, 6207 (1985).
- [14] R. de Picciotto, H. L. Stormer, L. N. Pfeiffer, K. W. Baldwin, and K. W. West, Nature **411**, 51 (2001).
- [15] S. J. Tans, M. H. Devoret, H. Dai, A. Thess, R. E. Smalley, L. J. Geerligs, and C. Dekker, Nature **386**, 474 (1997).
- [16] H. W. C. Postma *et al.*, Science **293**, 76 (2001).
- [17] A. Javey *et al.*, Nature **424**, 654 (2003).
- [18] Z. Chen *et al.*, Nano Lett **5**, 1497 (2005).
- [19] F. Schwierz, Nature Nanotech. **5**, 487 (2010).
- [20] J. P. Llinas *et al.*, Nature Comm. **8**, 633 (2017).
- [21] T. Markussen, R. Rurali, A.-P. Jauho, and M. Brandbyge, Phys. Rev. Lett. **99**, 076803 (2007).
- [22] M. A. Novotny, Phys. Rev. B **90**, 165103 (2014).
- [23] G. Inkoom and M. A. Novotny, J. Phys. Commun. **2**, 115019 (2018).
- [24] K. Nakada, M. Fujita, G. Dresselhaus, and M. S. Dresselhaus, Phys. Rev. B **54**, 17954 (1996).
- [25] Y.-W. Son, M. L. Cohen, and S. G. Louie, Phys. Rev. Lett. **97**, 216803 (2006).
- [26] The Fourier transform of the disordered model can be performed, but the lack of translational invariance makes a physical association with the wavevector of an electron quasi-particle problematic.
- [27] S. Datta, *Electronic Transport in Mesoscopic Systems* (Cambridge University Press, Cambridge, UK, 1995).
- [28] D. K. Ferry and S. M. Goodnick, *Transport in Nanostructures* (Cambridge, Cambridge University Press, 1997).
- [29] T. N. Todorov, J. Phys. Cond. Matter **14**, 3049 (2002).
- [30] H. Haug and A.-P. Jauho, *Quantum Kinetics in Transport and Optics of Semiconductors*, 2nd ed. (Springer, Berlin, 2008).
- [31] K. Hirose and N. Kobayashi, *Quantum Transport Calculations for Nanosystems* (Pan Stanford Publishing, Singapore, 2014).
- [32] D. Daboul, I. Chang, and A. Aharony, Eur. Phys. J. B **16**, 303 (2002).
- [33] M. F. Islam and H. Nakanishi, Phys. Rev. E **77**, 061109 (2008).
- [34] A. E. Miroschnichenko, S. Flach, and Y. S. Kivshar, Rev. Mod. Phys. **82**, 2257 (2010).
- [35] U. Fano, Phys. Rev. **124**, 1866 (1961).
- [36] Unfortunately the literature typically uses $\epsilon_{i,j}$ for the tight binding on site energy and ϵ_{Fano} for the dimensionless distance from E_{Fano} , but they should not be confused since they are differentiated by the subscripts. Similarly, q_{Fano} is not a wavevector.
- [37] Although our discussion is valid for any material based on a 2D hexagonal lattice, for ease of argument we limit ourselves to only carbon materials since they have received the most study.
- [38] Y. Segawa, M. Kuwayama, Y. Hijikata, M. Fushimi, T. Nishihara, J. Pirillo, J. Shirasaki, N. Kubota, and K. Itami, Science **365**, 272 (2019).
- [39] *Mathematica, Version 12.0*, Champaign, IL (2019).
- [40] J. Campos-Delgado *et al.*, Chem. Phys. Lett. **469**, 177 (2009).
- [41] K. M. Liew, C. H. Wong, X. Q. He, and M. J. Tan, Phys. Rev. B **71**, 075424 (2005).
- [42] J. Molina-Duarte, L. I. Esinosa-Vega, A. G. Rodriguez, and R. A. Guirado-López, Phys. Chem. Chem. Phys. **19**, 7215 (2017).
- [43] H. Santos, L. Chico, and L. Brey, Phys. Rev. Lett. **103**, 086801 (2009).
- [44] V. Kosynkin, W. Lu, A. Sinitskii, G. Pera, Z. Sun, and J. Tour, ACS Nano **5**, 968 (2011).
- [45] T. Hasegawa and H. Kohno, Phys. Chem. Chem. Phys. **17**, 3009 (2015).
- [46] W. Liang, M. Bockrath, D. Bozovic, J. H. Hafner, M. Tinkham, and H. Park, Nature **411**, 665 (2001).
- [47] S. Tanda *et al.*, Nature **417**, 397 (2002).
- [48] E. W. S. Caetano, V. N. Freire, S. G. dos Santos, D.S.Galv ao, and F. Sato, J. Chem. Phys. **128**, 164719 (2008).
- [49] X. Wang, X. Zheng, M. Ni, I. Zou, and Z. Zeng, App. Phys. Lett. **97**, 123103 (2010).
- [50] A. Sadrzadeh, M. Hua, and B. Yakobson, App. Phys. Lett. **99**, 013102 (2011).
- [51] S.-Y. Yue, Q.-B. Yan, Z.-G. Zhu, H.-J. Cui, Q.-R. Zhen, and G. Su, Carbon **71**, 150 (2014).
- [52] X. Zhang, B. Tian, W. Zhen, Z. Li, Y. Wu, and G. Lu, J. Catalysis **354**, 258 (2017).
- [53] M. A. Novotny, J. Math. Phys. **20**, 1146 (1979).
- [54] The supplemental materials include a ReadMe file, one

- .pdf file, and fourteen .cdf files.
- [55] C. Kittel, *Introduction to Solid State Physics*, 7th ed. (John Wiley & Sons, New York, 1996).
- [56] N. W. Ashcroft and N. D. Mermin, *Solids State Physics* (Holt, Rinehards and Winston, New York, 1976).
- [57] P. Hofmann, *Solid State Physics: An Introduction* (Wiley-VCH, Weinham, Germany, 2015).
- [58] D. Fathi, *J. Nanotechnology* **2011**, 471241 (2011).
- [59] Y. Hancock, A. Uppstu, K. Saloriutta, A. Harju, and M. J. Puska, *Phys. Rev. B* **81**, 245402 (2010).
- [60] J. Cao, X. H. Yan, J. W. Ding, and D. L. Wang, *J. Phys. Cond. Matter* **13**, L271 (2001).
- [61] J. D. Correa, A. J. R. da Silva, and M. Pacheco, *J. Phys. Cond. Matter* **22**, 275503 (2010).
- [62] J. C. Charlier, X. Blase, and S. Roche, *Rev. Mod. Phys.* **79**, 677 (2007).
- [63] A. G. Cano-Márquez *et al.*, *Nano Lett.* **9**, 1527 (2008).
- [64] L. Jiao, L. Zhang, X. Wang, G. Diankov, and H. Dai, *Nature* **458**, 877 (2009).
- [65] D. V. Kosynkin *et al.*, *Nature* **458**, 872 (2009).
- [66] Z. Zhang *et al.*, *J. Am. Chem. Soc.* **131**, 13460 (2009).
- [67] A. L. Elias *et al.*, *Nano Lett.* **10**, 366 (2010).
- [68] F. Yu *et al.*, *Small* **9**, 2405 (2013).
- [69] Q. Peng *et al.*, *Adv. Mater.* **26**, 32413247 (2014).
- [70] W. E. Mahmoud, F. S. Al-Hazmi, and G. H. Al-Harbi, *Chem. Eng. J.* **281**, 192 (2015).
- [71] C. S. Tiwary *et al.*, *Carbon* **89**, 217 (2015).
- [72] Y. Cheng, S. Zhang, J. Li, J. Sun, J. Wang, C. Qin, and L. Dai, *RSC Adv.* **7**, 21953 (2017).
- [73] Q. Zhao, X. Gan, Q. Lei, W. Li, and K. Zhou, *Composite Interfaces* **10**, 1 (2020).
- [74] Y. Song, M. Feng, and H. Zhan, *Electrochem. Comm.* **45**, 95 (2014).
- [75] L. Li, L. H. Li, Y. Chen, X. J. Dai, P. R. Lamb, B.-M. Cheng, M.-Y. Lin, and X. Liu, *Angew. Chem. Int. Ed.* **52**, 4212 (2013).
- [76] C. Child, *Phys. Rev. (Series I)* **39**, 492 (1911).
- [77] I. I. Langmuir, *Phys. Rev.* **2**, 450 (1913).
- [78] G. Auton, J. Zhang, R. Kumar, *et al.*, *Nat. Comm.* **7**, 11670 (2016).
- [79] V. A. Kochelap, V. V. Korotyeyev, Y. Lyashchuk, and K. W. Kim, *J. Appl. Phys.* **126**, 085708 (2019).
- [80] Q. Diduck, M. Margala, and M. J. Feldman, *IEEE MTT-S International Microwave Symposium Digest*, 345 (2020).
- [81] P. Custer, J. D. Low, D. J. Hill, T. S. Teitsworth, J. D. Christesen, C. J. McKinney, J. R. McBride, M. A. Brook, S. C. Warren, and J. F. Cahoon, *Science* **368**, 177 (2020).
- [82] N. C. Harris, G. R. Steinbrecher, M. Prabhu, Y. Lahini, J. Mower, D. Bunandar, C. Chen, F. N. C. Wong, T. Baehr-Jones, M. Hochberg, S. Lloyd, and D. Englund, *Nature Photonics* **11**, 447 (2017).
- [83] L. Lorz, E. Meyer-Scott, T. Nitsche, V. Potoček, A. Gábris, S. Barkhofen, I. Jex, and C. Silberhorn, *Physical Review Research* **1**, 033036 (2019).
- [84] H. Tang, X.-F. Lin, Z. Feng, J.-Y. Chen, J. Gao, K. Sun, C.-Y. Wang, P.-C. Lai, X.-Y. Xu, Y. Wang, L.-F. Qiao, A.-L. Yang, and X.-M. Jin, *Science Advances* **4**, eaat3174 (2018).
- [85] D. Shemesh, *Linear Algebra and Its Applications* **62**, 11 (1984).
- [86] D. Arapura and C. Peterson, *Linear Algebra and Its Applications* **384**, 1 (2004).